UNIVERSITY OF SALERNO

DEPARTMENT OF INDUSTRIAL ENGINEERING

Ph.D. Course in Industrial Engineering
Curriculum in Mechanical Engineering - XXXIII Cycle

Topological quantum technologies

Supervisor
Prof. Fabrizio Illuminati

Ph.D. student
Antonio Marino

Scientific Referees
Dr. Vincenzo Alba
Dr. Marcello Dalmonte

Ph.D. Course Coordinator *Prof. Francesco Donsì*

ACADEMIC YEAR: 2019/2020

INDEX

ABSTRACT

Precision measurements through engineered quantum systems are achieving new primacies in sensitivity and accuracy and therefore novel potential applications ranging from mechanical and electrical engineering to material science, nano-medicine, environmental science, and, in general, frontiers of technological development at large. For instance, the one-electron transistors and the one-spin qubits have been used as single quantum probes to detect electrical fields with unprecedented levels of precision. On the other hand, sensing schemes based on single quantum systems are strongly vulnerable even to very low levels of noise, due to the fragility of quantum coherence and the extreme sensitivity of quantum coherent probes. Recent efforts in quantum sensing and quantum metrology address this issue resorting to decoupling techniques and quantum correction schemes with quantum control feedback loops. Unfortunately, the experimental complexity and the control and precision requirements of such correction schemes, are exceedingly demanding both with present-day and currently foreseeable technologies.

An alternative route is to aim for passive control strategies, for instance by considering quantum systems that are naturally robust against local sources of noise such as imperfections and localized perturbations. Symmetry-protected (SP) topological phases of matter are strong candidates for the realization of such strategy, as they are intrinsically robust against local noise of appropriate symmetry. However, even SP topological order remains very fragile against global environmental effects such as statistical noise and thermal excitations. The long-term aim of passive strategies is then to identify, characterize, and quantify the core features of topological phases in terms of their structure of nonlocal quantum correlations, in order to set the stage for future protection schemes against global sources of noise and decoherence. Considering symmetry-protected topological systems, the final goal is to effectively shield them from global noise by "trapping" low energy excitations and drastically reducing their mean free path to distances much smaller than the system size. This procedure would still preserve the topological nature of the system, at the same time making topological devices insensitive to levels of thermal noise manageable in the lab.

In this thesis work we report on the first part of this long-term project, namely the qualification, characterization, and quantification of topological order in terms of nonlocal quantum correlations. During the first and central parts of our PhD project we have performed a comparative study of the bulk and edge properties of topological and symmetry-breaking one-dimensional model Hamiltonians (Kitaev and Ising chains) at zero temperature. We have

introduced and applied for the first time a new measure of entanglement to quantum many-body systems, the squashed entanglement previously investigated in the framework of quantum information, and we have found that in SP topological chains the squashed entanglement between the chain's edges is maximal and localizes the entire quantum information in the topological phase, while for symmetry-breaking systems the edges are still entangled but the quantum information diffuses through the chain's bulk. During the last part of our PhD studies we have generalized this approach to the study of topological spin-1 chains and two-dimensional systems, obtaining preliminary results analogous to those found for the simplest 1-D systems. Using tools of quantum information ranging from quantum discord and quantum coherence to multipartite squashed entanglement and multipartite nonlocality, we will strive to assess the optimal framework making topological order most resilient against thermal noise for systems defined both in flat and artificially curved geometries, at zero and finite temperature, and both for equilibrium and out of equilibrium configurations.

INTRODUCTION

Matter presents itself in different phases. More than half a century ago, Landau developed a theory to describe phases of matter on the basis of the concept of symmetry breaking. He pointed out that the distinction between different phases stems from the way their constituent particles are organized (ordered); different phases correspond to different symmetries of the particles' ordering. For example, the symmetry-breaking theory describes what happens when water freezes into ice: whereas liquid water has rotational symmetry at the atomic scale (it looks the same in every direction), the H_20 molecules in ice are locked in crystalline lattice: in an ordered phase of matter certain symmetries are "spontaneously" broken. For many years, it was widely believed that the symmetry-breaking theory described all phases of matter and all phase transitions. Things changed in 1982 with the discovery of phases called fractional quantum Hall states in an ultracold, two-dimensional gas of electrons. These strange states of matter feature emergent particles with fractions of an electron's charge that accumulate fractional steps in a one-way march around the boundary of the system. As a consequence, topological systems behave like an ordinary electrical insulator in the bulk but have conducting states on their boundaries, i.e., edges, perimeters or surfaces, and thus they can conduct electricity on their very boundary. Conducting boundaries are a central feature, but alone they are not the only ingredient that makes topological materials unique; rather, the most striking aspect of topological phases is that, thanks to the fact that topological properties are global, the surface states are extremely robust and stable against local perturbations. The topological phases are associated to the topological degeneracy of the lowest energy states, the so-called ground states, and therefore tend to manifest themselves only near absolute zero, because only at such low temperatures can systems of particles settle into their lowest-energy states. In the ground state, the delicate interactions that correlate particles' identities link up particles in global patterns of long-range quantum entanglement. Instead of having individual mathematical descriptions, particles become components of a more complicated function that describes all of them at once, often with entirely new particles emerging as the excitations of the global phase.

Topological materials promise many potentially useful technological applications, such as more energy-efficient microelectronic components, better catalysts, improved thermoelectric converters, or new magnetic storage media and logical memories robust against local sources of noise, imperfections and perturbations. In fact, in quantum metrology schemes based on single quantum systems, the challenge that needs to be overcome is the

strong vulnerability to noise associated with such sensitive probes. Recent work into quantum metrology schemes that make use of quantum error correction and decoupling techniques [1-8] attempt to address this issue. The control requirements and experimental complexity for such schemes, however, are quite daunting with current experimental techniques. Metrological schemes based on topological quantum devices would not suffer from these shortcomings, as they would be intrinsically protected from the detrimental effects of local noise, imperfections, and perturbations. In order for topological devices to become a concrete reality it is necessary to develop methods for the preliminary assessment, characterization and quantification of topological order, and for its detections.

The aim of our research work is to propose methods able both to quantify and to discriminate topological systems from symmetry-breaking ones, and that are amenable to experimental verification. This thesis report is divided in three parts: in the first part (chapter 1) we describe the state of the art of topological systems and the mathematical techniques that we will use to study them. In the second part (chapter 2) we review different approaches to the realization of useful topological quantum technologies. In the third part (chapter 3) we illustrate the goals of the project, we describe the research activity developed during the PhD course and the results obtained, and we discuss several follow-up lines of research for future investigations.

LIST OF FIGURES

- Figure II.6: (a) Behaviour of centre of mass of pumped charge in function of time for different trajectories, (b), (c),(d), (e) Energy gap of systems for different values of winding numbers .

- Figure III.1 Examples of tripartitions (a) and quadripartitions (b) in Ising (left) and Kitaev (right) chains of finite size with open boundary conditions. A and B denote the two edges, while C denotes the bulk and C_1 and C_2 denote the two halves (not necessarily symmetric) of the same bulk C.

- Figure III.2 Behaviour of the bipartite edge-edge squashed entanglement $\mathcal{E}_{sq}^{ee}(\rho_{AB})$ of the two-edge state ρ_{AB} for the open Ising chain as a function of the external field h and for the open non-interacting Kitaev chain as a function of the chemical potential μ. Panels (a), from left to right: Ising and Kitaev edge-edge squashed entanglement for the (ACB) tripartition edge-bulk-edge and different chain lengths (L = 10, 12, 14). Panels (b), from left to right: Ising and Kitaev edge-edge squashed entanglement for the (AC_1C_2B) quadripartition edge-bulk-bulk-edge and different chain lengths (Ising: L = 14; Kitaev: L = 10, 12, 14). Red lines: L = 10; green lines: L = 12; blue lines: L = 14.

- Figure III.3 Behaviour of the bipartite edge-bulk squashed entanglement $\mathcal{E}_{sq,3}^{eb}(\rho_{AC}) = \mathcal{E}_{sq,3}^{eb}(\rho_{BC})$ for the open Ising chain (L = 8,10,12) and the open non-interacting Kitaev chain (L = 8) for the (ACB) tripartition edge-bulk-edge. The results have been obtained by exact numerical diagonalization using an optimized Mathematica package.

- Figure III.4 Behaviour of the edge-edge bipartite squashed entanglement in the Ising and in the non-interacting Kitaev open chains for: (a) the tripartition edge-bulk-edge (ACB) and chain size L = 10,12,14 for both models; and for: (b) the quadripartition edge-bulk-bulk-edge (AC_1C_2B) and chain size L = 14 for the Ising system and L = 10, 12, 14 for the Kitaev system. Red line: L = 10; green line: L = 12; blue line: L = 14. The results have been obtained numerically using Mathematica package.

- Figure III.5 Comparison of Fidelity for the Ising chain and the non-interacting Kitaev chain for L = 10. Red curve: normal edges, blue curve: diamagnetic edges. The results have been obtained numerically with Mathematica package.

- Figure III.6 Comparison of the edge-edge squashed entanglement in the interacting Kitaev chain vs. the end-to-end entanglement in the XYZ spin-1/2 chain, illustrated for a size of the system L=4. In analogy with the non-interacting case, the edge-bulk-edge leads to no discrimination, while the edge-bulk-bulk-edge quadripartition fully discriminates between the symmetric topological order and the symmetry-breaking Ginzburg-Landau order. In comparison with the non-interacting case, we see that the interaction stabilizes the edge-to-edge entanglement throughout almost the entire topological phase

- Figure III.7: Tripartition edge-bulk-edge for a quantum lattice model with two edges on both end sides of a one-dimensional open chain of finite size L.

- Figure III.8 Behaviour of the squashed entanglement in the ground state of a cluster spin model and of the corresponding symmetry-breaking counterpart, for a finite open chain of length L = 9. Panel (a): edge-edge squashed entanglement for a tripartition (ACB). No detectable difference between the two models. Panel (b): edge-bulk squashed entanglement in the two models. Blue curve: cluster spin model with symmetry protected topological order: vanishing entanglement. Red curve: symmetry-breaking counterpart with standard Ginzburg-Landau magnetic order. The edge-bulk squashed entanglement discriminates between the two models at the tripartite level, proving the topological nature of the model.

- Figure III.8bis Panel (a): Behaviour of the edge-edge squashed entanglement for a quadripartition (AC_1 C_2 B) in the ground state of a cluster spin model for a finite open chain of length L = 9. Panel (b): Behaviour of the edge-edge squashed entanglement for the same quadripartition (AC_1 C_2 B) in the ground state of the symmetry-breaking counterpart model for a finite open chain of length L = 9. The edge-edge squashed entanglement is finite throughout the entire topological phase of the cluster spin chain (no edge-bulk correlation), and is vanishing in all phases of the symmetry-breaking counterpart model (non-vanishing edge-bulk correlation); it thus discriminates between the two models and reveals the (symmetry-protected) topological nature of the 1-D cluster spin model, in complete analogy with the previous comparative investigation of the Kitaev fermionic chain vs the Ising spin chain.

- Figure III.9 Edge-edge squashed entanglement in the ground state of the 1-D cluster spin model on an open chain of size L = 9 as a function of the external field h. Red curve: cluster spin chain with diamagnetic edges; Blue curve: cluster spin chain without diamagnetic edges. The diamagnetic edges stabilize the topological entanglement at the constant maximum value ln(2) throughout the entire topological phase (h < 1).

- Figure III.10 Sawtooth open chain lattice of finite size. The two constituent sublattices A and B are endowed with exchange interactions, respectively of strength J1 = 1 and J2 = D, denoted by the grey and the green segments.

- Figure III.11 Edge-bulk squashed entanglement as a function of the external field h for an Heisenberg-like Hamiltonian, Eq. (III.49), on an open sawtooth chain with L = 9 sites, with an edge-bulk-edge tripartition (ACB), for different values of the sublattice interaction strength D. Panel (A) D = 0.5. Panel (B): D = 0.5. Panel (C): D = 1.5. We see that for a value of D above a critical threshold D_(c) the bulk becomes conducting and gets correlated with the chain edges, barring the onset of a topological phase.

- Figure III.12 A toric-code model defined on a lattice of seven spins ½ (X.-G. Wen and collaborators in the book "*Quantum Information Meets Quantum Matter*" by Bei Zeng, Xie Chen, Duan-Lu Zhou, and Xiao-Gang Wen (Springer, NY, 2019))

- Figure III.13 Ground-state squashed entanglement for a toric-code Hamiltonian model defined on a two-dimensional lattice of L = 7 spins on the bonds, with periodic boundary conditions. Panel (a): edge-edge squashed entanglement obtained for a canonical edge-bulk-edge tripartition (ACB). Panel (b): edge-bulk squashed entanglement for the same tripartition. We see that the edge-edge entanglement is non vanishing while the edge-bulk entanglement is identically zero, thus corresponding to a bona fide topological phase of the system.

- Figure III.14 Ground-state squashed entanglement for a toric-code Hamiltonian model defined on a two-dimensional lattice of $L = 7$ spins on the bonds, with periodic boundary conditions. Panel (a): edge-edge squashed entanglement obtained for a canonical edge-bulk-edge tripartition (ACB) and diamagnetic edges. Panel (b): same edge-edge squashed entanglement for the same tripartition, and diamagnetic bulk. We see that the edge-edge entanglement is stabilised by the diamagnetic edges throughout the entire topological phase, while it remains insensitive even to a diamagnetically modified bulk.

Chapter 1
Topological order and entanglement

I.1 Issues concerning a macroscopic definition of topological order

The known symmetry-breaking order is defined by some physical concepts that allow us to identify and characterize them via experimental protocols and/or numerical calculations. For example, the concept of superfluid order is defined by zero viscosity and the quantization of vorticity, and the concept of crystal order is defined by X-ray diffraction experiments. The viscosity and X-ray diffraction are linear responses easily measurable in experiments and the type of order that they identify is easy to understand. However, the topological order is a peculiar and elusive order that cannot be determined by any linear response. Rather, in the early stages, before the "entanglement revolution" came about, it was surmised that topological order is singled out by:

a) Topological ground state degeneracy on closed spaces of various topologies;

b) Non-Abelian geometric phases of those degenerate ground states arising from space deformations.

Topological degeneracy is associated to ground-state degeneracy[1] of quantum gapped many body systems[2] in the large system size limit (large but strictly finite). The topological degeneracy has the following properties:

a) It is never exact, but for a set of some special points of exact topological degeneracy. However, the energy gap closes exponentially with the (finite) size of the system.

b) Topological degeneracy is stable against local perturbations.

c) Topological degeneracy is removed in the thermodynamic limit (as there is no boundary, and thus no topology).

The topological degeneracy for a given system usually is different for different space topologies. For example, for a Z_2topological order in one dimension, the topological degeneracy is $D_g = 2$, while for $Z_2 \times Z_2$ topological order $D_g = 4$.

From the above examples one can attribute the topological ground state degeneracy to specific symmetries. At the same time, the ground state degeneracy is robust against any local perturbation that breaks all symmetries. Moreover, topological order can occur only for finite-size systems, at variance with systems possessing symmetry-breaking order. Indeed, for the latter, exact ground-state degeneracy can strictly occur only in the thermodynamic limit (there are finite-size exceptions at very special points, such as factorization points). Therefore, topological degeneracy is a rather peculiar phenomenon that implies a new type of order, very different from symmetry-breaking order.

Ground state degeneracy is not sufficient to characterize completely topological order, especially in D=2 and higher dimensions. Indeed, there can exist different topological orders with the same ground state degeneracy. The non-Abelian geometrical phases are quantum numbers that characterize completely the topological order. They are obtained with a deformation of background space where is placed the many body topological system. For

[1] Two or more pure states of a quantum mechanical system are said to be degenerate if they are energy eigenstates (eigenstates of the system' Hamiltonian operator H) corresponding to the same energy eigenvalue.

[2] Very loosely speaking, a quantum systems is gapped if there exists a finite energy separation between the ground state and the excited states. In the instance of systems of infinite size (i.e., in the so-called thermodynamic limit), a system is gapped if the ground-state degeneracy of the Hamiltonian H is upper bounded by a finite integer, and the energy gap Δ between the ground state(s) and the first excited state(s) of H is lower bounded by a finite positive number.

example, we consider a many body system on a torus and perform a "shear" deformation of the torus, mathematically represented by unitary matrix, from which we can obtain a one parameter family of gapped Hamiltonians H_g ($g \in [0,1]$) that form a loop (i.e. $H_0 = H_1$). The non-Abelian geometrical phases obtained in this way are denoted as T phases. In addition, we can generate a "squeezing" deformation of the tours obtaining another non-Abelian geometrical phase denoted S. The phases T and S contain information about the topological properties of the topological ordered states, such as fractional statistics.

I.2 Quantum correlations and entanglement

Intuitively, correlations describe the dependence of certain properties on the interaction of different parts of a composite system. It is thus very important to characterize correlations, both qualitatively and quantitatively. Correlations can be characterized in different ways. For example, for many body systems, correlations are usually expressed in terms of correlation functions of the type: $< O_i O_j > - < O_i >< O_j >$, where $< O_i >$ denotes the expectation value of observable O_i on the site i with respect to the quantum state of the system. The behaviour of correlation functions provides useful information such as the correlation length for phase transitions.

Correlations are not the end of the story when it comes to quantum phase transitions. In fact, one of the central traits (if not the central trait) of quantum mechanics is the superposition principle and the ensuing linearity of the theory: "every quantum state can be represented as a linear combination of two or more other distinct states". The superposition principle of quantum mechanics is responsible for the onset of a very peculiar type of correlation: quantum entanglement. Let us consider a bipartite system composed by subsystems A and B, respectively with Hilbert spaces H_A and H_B. The Hilbert space of a composite system made of distinguishable subsystems (the situation is more complicated in the case of indistinguishability, and one needs to resort to the concept of quotient space) is the tensor product of the individual spaces: $H_A \otimes H_B$. If the first system is in pure state $|\psi_A\rangle$ and the second in pure state $|\phi_B\rangle$, the state of the composite system is then:

$$|\psi_A\rangle \quad \otimes \quad |\phi_B\rangle \qquad (\mathrm{I}.1).$$

States of the composite system that can be represented in this form are called separable states, or product states. They are not entangled, and they are uncorrelated.

Not all states are separable states (and thus product states in the case of pure states). Given a basis $\{|i_A\rangle\}$ for H_A and a basis $\{|j_B\rangle\}$ for H_B, the most general pure state in $H_A \otimes H_B$ is of the form:

$$|\Psi_{AB}\rangle = \sum_{i,j} c_{ij}|i_A\rangle \otimes |j_B\rangle \qquad \text{(I. 2).}$$

This state is separable if there exist some (Schmidt) coefficients c_i^A, c_j^B so that $c_{ij} = c_i^A\, c_j^B$. It is not separable if for one pair of constants c_i^A, c_j^B we have $c_{ij} \neq c_i^A\, c_j^B$. If a state is not separable, it is called an 'entangled state'.

For example, take the case of a two-qubit (two spins 1/2) system and fix two basis vectors $\{|0_A\rangle, |1_A\rangle\}$ of H_A, and two basis vectors $\{|0_B\rangle, |1_B\rangle\}$ of H_B the following state is an entangled state:

$$\frac{1}{\sqrt{2}}(|0_A\rangle \otimes |1_B\rangle - |1_A\rangle \otimes |0_B\rangle) \qquad \text{(I. 3).}$$

If the composite system is in this state, it is impossible to attribute to either subsystem A or subsystem B a definite state. Another way to say this is that while the von Neumann entropy[3] of the whole state is zero (the von Neumann entropy of a pure state, i.e. a projector, is always zero), the entropy of any of the two subsystems is greater than zero, as any subsystem of an entangled pure state is in a mixed state (reduced density matrix). In this sense, the subsystems are "entangled". The above example is one of four Bell states, which are (maximally) entangled pure states (pure states of the $H_A \otimes H_B$ space, but which cannot be separated into pure states of each H_A and H_B).

[3] For a quantum-mechanical system in a state described by a density matrix ρ , the von Neumann entropy is $S = -Tr(\rho ln \rho)$, where $Tr(..)$ is the trace operator.

In the last decade the understanding of correlations and quantum phase transitions in many-body systems has significantly improved thanks to the analysis and the study their entanglement properties [24-25].

I.3 Intuitive pictures of topological order: long-range entanglement

We can use dance to give an intuitive description of entanglement between particles in topological systems and we can evidence the different ways of dancing between particles that belong to symmetry-breaking system or topological system. In the symmetry breaking orders, every particle/spin (or every pair of particles/spins) dance by itself, and they all dance in the same way. For example, in a ferromagnet, every electron has a fixed position and the same spin direction. Instead, a topological order is described by a global dance, where every particle (or spin) is dancing with every other particle (or spin) in a very organized way: all spins/particles dance following a set of local dancing "rules" trying to lower the energy of a local Hamiltonian. As a consequence, the particles form a global dancing pattern that generates correlations which correspond to a pattern of long-range quantum entanglement. The long-range entanglement produces characteristic proprieties of topological order that are:

a) Quasiparticles with fractional statistics and fractional quantum numbers that also provide us ways to experimentally detect topological order;

b) Gapless boundary excitations in symmetry protected topological (SPT) systems (see section I.4) and gapped excitations in other topological systems such as the quantum dimer model on triangular lattice. These topological edge modes lead to perfect conducting boundaries, even in the presence of impurities. This property may lead to important topological devices for technological applications.

I.4 Symmetry-protected topological phases in 1D systems

Symmetry protected topological (SPT) phases are gapped quantum phases with topological properties protected by symmetry. The presence of symmetry causes the nontrivial SPT order with the existence of gapless edge states on the boundary of the system which cannot be removed as long as symmetry is not broken.

Here we introduce some simple 1-D examples of nontrivial SPT orders. The Kitaev fermionic chain is a one-dimensional tight-binding model for spinless fermions in the presence of p-wave superconducting pairing [9]. This model possesses a topological phase with two-fold-degenerate ground states that cannot be distinguished by any local order parameter. The Majorana zero-energy modes (quasi-particles generated by the fermion correlation) [10-14] are exponentially localized near the boundaries. The Hamiltonian operator for the non-interacting Kitaev chain of length L is:

$$H_K = \sum_{j=1}^{L-1}\left[-t\left(c_j^{+}c_{j+1} + c_{j+1}^{+}c_j\right) + \Delta\left(c_j c_{j+1} + c_{j+1}^{+}c_j^{+}\right)\right] - \frac{1}{2}\sum_{j=1}^{L}\mu\left(2c_j^{+}c_j - 1\right) \quad , \qquad (\text{I. } 4)$$

where c_i^{+} and c_i are the creation and annihilation operators, respectively, t is the hopping amplitude, Δ is the p-wave paring gap, which is assumed to be real, and μ is the chemical potential. For $\Delta = t$ and $\mu \leq 2t$, the system is in the topological phase, while for $\mu \geq 2t$, the system is in the trivial phase (band insulator). In particular for $\mu = 0$, the ground state is exactly two-fold degenerate and it is possible to show that the ground state is factorized. We consider the following definition:

$$c_j^{\pm} = \frac{1}{2}\left(\gamma_j^A \pm i\gamma_j^B\right) \qquad (\text{I. } 5),$$

where γ_j^A and γ_j^B are the self-adjoint Majorana operators. One can easily see that they satisfy the defining relations:

$$\left\{\gamma_j^A, \gamma_k^B\right\} = 0, \qquad (\text{I. } 6).$$

$$\left\{\gamma_j^A, \gamma_k^A\right\} = \left\{\gamma_j^B, \gamma_k^B\right\} = 2\delta_{jk}$$

Substituting the formula (I.5) in (I.4) we have the following Hamiltonian for $\mu = 0$ and $\Delta = t$:

$$H_K = 2it \sum_{j=1}^{L-1} \gamma_{j+1}^A \gamma_j^B \qquad (\text{I}.7).$$

We can see that the two end Majorana modes γ_1^A and γ_L^B do not appear in H_K at all. Hence our chain has two zero-energy states, localized at its ends. All the states which are not at the ends of the chain have an energy of $\pm|t|$, independently on the length of the chain. Hence, we have a one-dimensional system with a gapped bulk and zero energy states at the edges. This degeneracy is an example of topological degeneracy because it is protected by a topological invariant. Since the topological invariant comes from a particle-hole symmetry which is a discrete symmetry, such topological order has been called symmetry-protected topological order.

Another interesting topological quantum many-body system in one dimension is the spin-1/2 cluster model, whose Hamiltonian is:

$$H_c = -\sum_{j=2}^{L-1} \sigma_{j-1}^x \sigma_j^z \sigma_{j+1}^x - h \sum_{j=1}^{L} \sigma_j^z \qquad (\text{I}.8),$$

where σ_j^x, σ_j^z are the Pauli matrices and h is an external magnetic field. The ground state, for h = 0, is exactly 4-fold degenerate. The degeneracy is caused by the symmetry group $D_2 = Z_2 \times Z_2$. Any local perturbation respecting the symmetry cannot lift the ground state degeneracy for finite-size systems. In this sense, the system is said to have "symmetry-protected topological (SPT) order".

A very important spin-1 topological model in one dimension is the Affleck-Kennedy-Lieb-Tasaki (AKLT) chain, whose bilinear biquadratic Hamiltonian reads:

$$H_{AKLT} = \sum_{i=1}^{L-1} S_i S_{i+1} + \frac{1}{3}(S_i S_{i+1})^2 \qquad \text{(I. 9)},$$

where S is the spin 1 operator. This Hamiltonian is invariant under the SO(3) spin rotation symmetry. It is a particular, exactly solvable, case of the Haldane Heisenberg chain for spin 1. We can give the following representation of AKLT chain:

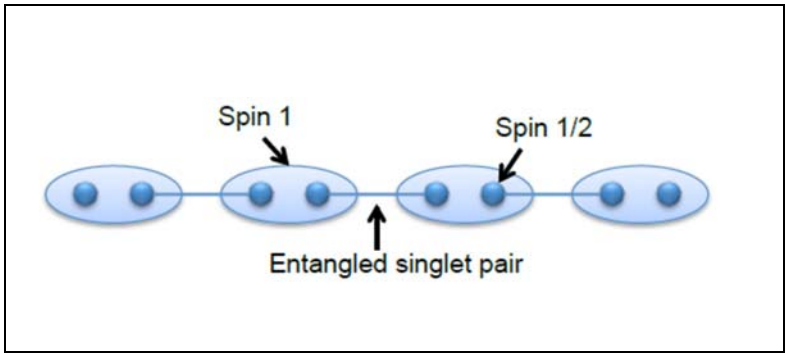

Figure I.1 *AKLT chain*

Each lattice site (big oval) contains two spin 1/2s (small circle), which form singlet pairs (connected bonds) $|{\downarrow\uparrow}\rangle - |{\uparrow\downarrow}\rangle$ with another spin 1/2 on a neighbouring site. By projecting the two spin 1/2 on each lattice site to a spin 1, we obtain the ground state wave function. There are isolated spin 1/2 at each end of the chain which are not coupled with anything and give rise to a two-fold degenerate edge state. The full ground state on an open chain is hence four-fold degenerate. The degenerate edge state is stable as long as spin rotation symmetry is preserved.

I.5 How to identify topological order via quantum entanglement?

From the previous discussion, topological order appears to be characterized by the entanglement between quasi-particle localized at the chain boundaries. How can we quantify the entanglement between the edges of the system?

A legitimate entanglement monotone E must satisfy the following proprieties:

a) It must vanish on separable states: $E\left(\rho = \sum_k c_k \rho_A^k \otimes \rho_B^k\right) = 0$.

b) It must not increase under the action of local operations and classical communication: $E(K\rho K^{-1}) \leq E(\rho)$.

c) It must remain invariant under local unitary operations: $E\left(U\rho U^{\dagger}\right) = E(\rho)$.

Properties a) through c) above make up the very minimal set of properties any legitimate entanglement quantifier must satisfy. An entanglement monotone E is promoted to a full entanglement measure Ɛ provided the following additional properties are satisfied:

d) Convexity: $E(\lambda\rho_1 + (1-\lambda)\rho_2) \leq \lambda E(\rho_1) + (1-\lambda)E(\rho_2)$.

e) Additivity: $E(\rho_A \otimes \rho_B) \leq E(\rho_A) + E(\rho_B)$.

f) Continuity: If $||\rho - \sigma|| \to 0\ then\ |E(\rho) - E(\sigma)| \to 0$.

g) On pure states, E must reduce to the von Neumann entanglement entropy of the reduced density matrix.

h) On multipartite systems, E should be monogamous: $E(A|BC) \geq E(A|B) + E(A|C)$.

Among the very many entanglement monotones and measures that have been introduced in the last decades, essentially only one satisfies all the above properties, namely the so-called squashed entanglement.

Let ρ_{AB} be a quantum state on a bipartite Hilbert space $H = H_A \otimes H_B$. The squashed entanglement of ρ_{AB} is defined as:

$$\mathcal{E}_{Sq}(\rho_{AB}) := inf\left\{\frac{1}{2} I(A;B|E):\ \rho_{ABE}\ is\ an\ extension\ of\ \rho_{AB}\right\} \quad (I.10).$$

The infimum is taken over all extensions of ρ_{AB} , i.e. quantum states of higher dimension ρ_{ABE} such that $\rho_{AB} = Tr_E(\rho_{ABE})$.

The quantity $I(A;B|E) = S(\rho_{AE}) + S(\rho_{BE}) - S(\rho_{ABE}) - S(\rho_E)$ is the so-called quantum conditional mutual information of state ρ_{ABE}, and in all the above formulas $S(\rho_x)$ denotes the von Neumann entropy of the underlying state.

In particular, if ρ_{ABE} is a pure state (a projector), then $I(A;B|E) = S(\rho_{AE}) + + S(\rho_{BE}) - S(\rho_E) = S(\rho_B) + S(\rho_A) - S(\rho_E)$, and one understands the origin of the nomenclature: quantum entanglement between A and B is what is left after the quantum correlations between E and the compound AB, quantified by $S(\rho_E)$, have been "squashed out" from the sum of the quantum correlations between A and the compound BE, quantified by $S(\rho_A) = S(\rho_{BE})$, and the quantum correlations between B and the compound AE, quantified by $S(\rho_B) = S(\rho_{AE})$, and one has taken the infimum over all possible extensions ρ_{ABE}.

The computational problem appears to be intractable in general, unless the extensions ρ_{ABE} form a restricted set fixed a priori by the physics of the system, as we will see in Chapter 3. Equally important, the squashed entanglement is amenable to experimental quantification in the lab, being a combination of entanglement entropies that can be measured with interferometric techniques [15] using quantum interference of many-body twins states: the parity expectation number of particles measures the quantum state overlap between two states, that is in turn directly connected to the von Neumann entropy. If experimentally measurable squashed entanglement relates to topological order, then it can be used to guide and assess the development of topological devices for quantum technologies. Let us then turn briefly to a description of the current state and perspective of topological quantum technologies.

Chapter 2
TOPOLOGICAL QUANTUM TECHNOLOGIES

II.1 Introduction

Building and implementing useful quantum technologies and quantum engineering has proved difficult, because of nearly inevitable interactions with the environment that cause decoherence[4] e.g. thermal fluctuations, stray fields, local noise, local perturbations and imperfections.

Practical methods of detecting and correcting errors have been devised (active approach). In recent article published in Science Advanced [16] researchers at the Joint Quantum Institute tested a full procedure for encoding a qubit[5] and detecting some of the errors that occur during and after the encoding. However, there are limitations to this approach. In fact, it is impossible to detect two consecutive errors and moreover locating an error precisely require more qubits, so it is very difficult to implement experimentally an error-correction feature.

Other approaches (passive) that do not require auxiliary qubits or measurements, they can be used as economical alternative to complement quantum error correcting codes. They consist in engineering quantum systems intrinsically immune to errors and resilient to decoherence. An example is the dynamical decoupling method [17], which aims to reduce decoherence times by attenuating the system-environment interaction. In dynamical decoupling, a sequence of control fields is periodically applied to a system in cycles of period τ_c, in order to refocus the system-environment evolution. However, systems with fast fluctuating environment are difficult to implement experimentally. They may be encountered in a wide range of quantum information processing implementations [18] and represent the most challenging regime for avoiding decoherence.

[4] Decoherence can be viewed as the loss of information from a system into the environment (often modelled as a heat bath), since every system is loosely coupled with the energetic state of its surroundings.

[5] A qubit is a two-state (or two-level) quantum-mechanical system.

In recent years, modern metrology and sensors are using topological materials of different nature and in different ways to build robust devices against local imperfections and errors. The spin chains, previously described in chapter one, are robust against local noise and imperfections. The noise sources are represented by invariant operator respect to the symmetry group that protects the topological order. Although these systems are less robust than the "fully topological" models, they have numerous advantages:

- They can be easily engineered in the laboratory;
- Quantum information can be transported robustly in any topological phase;
- The symmetry group can be used as a "handle": it is possible to manipulate the quantum information modelling the local interactions.

From a quantum point of view, they have some advantages respect to classical devices:

- More powerful than today's faster devices: they can store a lot of information (e.g. quantum computing, quantum simulation, quantum cryptography);
- High-precision measurements: quantum sensor can discriminate very weak signals with amplitude level at the Heisenberg limit, which is much lower than the classical noise threshold (Shot noise) (e.g. quantum metrology and quantum sensing)

In this chapter we report some fundamental experiences where topological materials are used to construct a classical and quantum device.

II.2 Topological classical devices

Recent studies have revealed that despite its apparent simplicity, this minimal setup is sufficient to construct topologically protected classical systems that mimic the properties of their quantum analogues. This follows from the fact that, irrespective of its classic or quantum nature, a periodic material with a gapped spectrum of excitations can display topological behaviour as a result of the nontrivial topology of its band structure.

The first experience, that we describe, is the construction of a robustness laser with a topological insulator material [30]. The purpose of the experience is to build a topological laser that is able to improve its efficiency by increasing its intensity. This is achieved by means of a system consisting of a laser beam that must pass through a suitably constructed plate capable of generating resonance effects that enhance the intensity of the laser beam itself. The plates are constructed using a topological material once in the topological phase and once in the trivial phase. The architecture of the plates is very complex but it is done in such a way as to generate a transport based on the topological edge-modes of the material. These edge-modes generate optical resonators due to a different chirality of the edge particles. If the topological plate is considered, the laser light that is sent from the outside undergoes single-mode constructive interference effects (i.e. there is only one resonant frequency between all the perimetral edges) which enhances the signal received from the outside, even if long local imperfections are inserted in the perimeter. The plate in the trivial phase does not give the same results as the external laser beam suffers different constructive or destructive interference. In fact, since the edge-modes are no longer present along the perimeters of the plates, the laser beam is emitted at different resonance frequencies, thus causing an attenuation of its intensity.

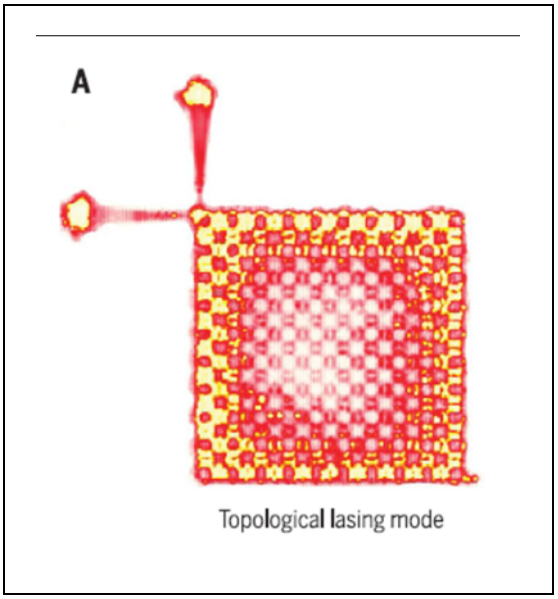

Figure-II.1 *Top-view image of the lasing pattern (topological edge mode) in a 10 unit cell–by–10 unit cell array of topologically coupled resonators and the output ports*

Nasha et al. [31] have built a new type of mechanical metamaterial: a "gyroscopic metamaterial" composed of rapidly spinning objects that are coupled to each other. In particular Topological mechanical metamaterials are artificial structures whose unusual properties are protected very much like their electronic and optical counterparts. At the edges of these materials, we find sound waves that are topologically protected (i.e. they cannot be scattered backward or into the bulk). These waves, which propagate in one direction only, are directly analogous to edge currents in quantum Hall systems. Through a mathematical model, they interpret the robustness of these edge waves in light of the subtle topological character of the bulk material. Breaking the time-reversal symmetry changes the distribution of angles at the edges of the honeycomb lattice. This geometric distortion of the lattice generates the topological effect of the edge-modes. The same topological effect is repeated if the gyroscopes are coupled by elastic springs. In this case the system is analogous to a Haldane spin chain in a honeycomb lattice.

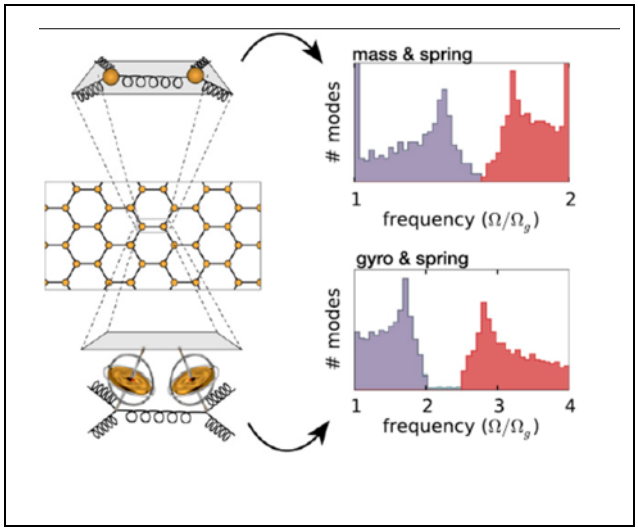

Figure-II.2 *A comparison between the density of states of a mass–spring (Top) and gyroscopic metamaterial on a honeycomb lattice. In both networks neighbouring masses (gyroscopes) are coupled by springs and each mass(gyroscope) feels a restoring force toward its equilibrium position.*

Ningyuan et a. [32] demonstrate the first simultaneous site- and time-resolved measurements of a time-reversal invariant topological band structure, which we realize in a radio-frequency photonic circuit. There are a variety of ways to engineer topologically nontrivial band structures in lattice models, which may be classified either as time-reversal-symmetry conserving or breaking. Among the time-reversal-breaking models, the simplest arises when a constant magnetic field is applied to a charged particle confined in a two-dimensional periodic structure. The time-antisymmetric Lorentz force is equivalent to an Aharanov-Bohm phase (flux) per plaquette $\phi = \frac{2\pi M}{N}$ (for relatively prime integers M, N). This flux breaks the intrinsic translational invariance of the lattice, resulting in an effective unit cell of size N sites and N corresponding sub-bands. To realize magnetic-field-like physics, they generate spin-orbit coupling through local circuit connections (Fig. II.3). We observe a gapped density of states consistent with a modified Hofstadter spectrum at a flux per plaquette of $\phi = \frac{\pi}{2}$. In situ probes of the band gaps reveal spatially localized bulk states and delocalized edge states. Time-resolved measurements reveal dynamical separation of localized edge excitations into spin-polarized currents. The radio-frequency circuit paradigm is naturally compatible with nonlocal coupling schemes, allowing us to implement a Möbius strip topology inaccessible in conventional

systems. This room-temperature experiment illuminates the origins of topology in band structure, and when combined with circuit quantum electrodynamics techniques, it provides a direct path to topologically ordered quantum matter.

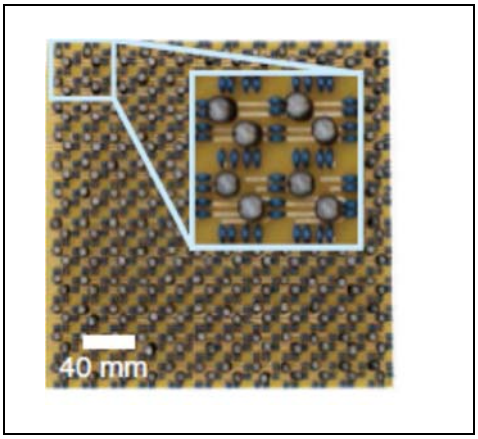

Figure-II.3 *Photograph of circuit topological insulator. The inductors (black cylinders) are coupled via the capacitors (blue); circuit topology is determined by the trace layout on the printed circuit board (yellow). Inset: Zoom-in view of a single plaquette consisting of four adjacent lattice sites.*

II.3 Measuring the direction of an unknown electric field

The group of Bartlett et al. [19] has used the Haldane chain to model spin 1 interacting bosonic particles. The chain preserves the rotations in Euclidean space (SO(3) symmetry group). Experimentally the Haldane chain is engineered using Rydberg atoms trapped in an optical lattice having a reticular pitch of a few micrometres. The interaction between the first neighbours is generated with laser beams in such way to bring Rydberg atoms towards excited states and to induce a dipole momentum.

The interaction between the first neighbours is generated with laser beams in such way to bring Rydberg atoms towards excited states and to induce a dipole momentum. The metrological scheme uses the entanglement between the edges of the chain (in topological phase) to measure the direction of an unknown electrical field, which destroys the symmetry group SO (3), but preserves the degeneration of the ground-state and therefore the topological order. In particular an edge is isolated adiabatically from the chain and it is coupled to the external field through a plane rotation of π along the direction of the field.

The information is transferred to the rest of the chain through the entanglement with the other edge.

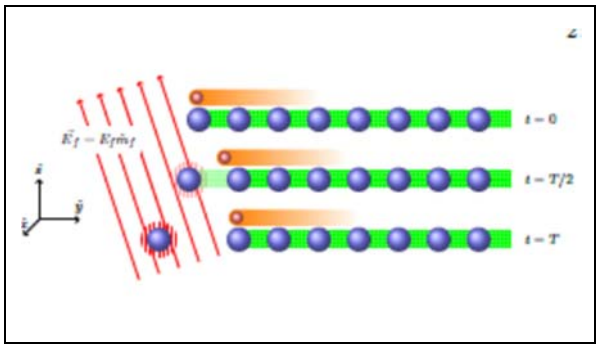

Figure-II.4- *Basic action of the sensing operation. Large (blue) spheres denote the spins of the chain. The left edge carries a fractionalized edge degree of freedom (orange). Adiabatically decoupling the boundary spin from its immediate neighbour while simultaneously subjecting it to interaction with the local field (red), transfers the encoded information to the slightly shorter chain.*

II.4 Topological optical interfaces

The experiment conducted by Barik et al. [20] presents a photonic device realized through the interface of two topological materials that have different properties. The main purpose of the work is to show that the device is able to transport light signals even in the presence of local disorder, obtained deforming the crystal lattice of the two materials by curvatures. They also show that the transport of signals is only due to the presence of two edge modes along the interface of the device with opposite polarization. Moreover, to highlight the different polarization of the two edges they send a magnetic field along the interface and record the signal emitted at the ends of the interface finding for each end a different polarization.

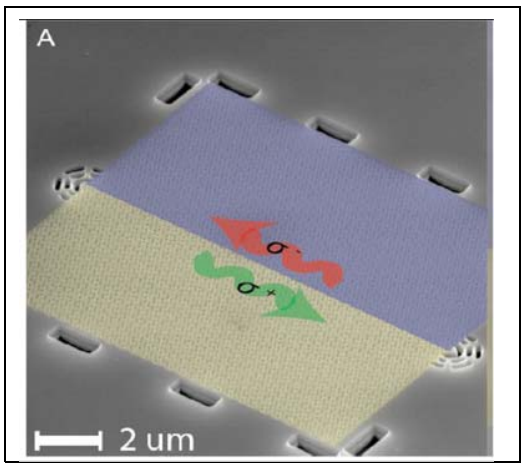

Figure -II.5- *The interface between the two photonic crystals supports helical edge states with opposite circular polarization.*

II.5 Realization of artificial magnetic fields in 2-D lattices

Stulh et al. [21] have realized a large artificial magnetic field engineering a two-dimensional lattice in an elongated strip geometry. They have used the localized edge and bulk states of atomic Bose-Einstein condensates in this strip. In fact, the constituent edge states can be viewed as skipping orbits which permit to acquired phases as atoms traversed the lattice. These phases take the place of the Aharonov-Bohm phases produced by true magnetic fields and suffice to fully define the effective magnetic field. This and related approaches have the technical advantage over other techniques for creating artificial fields in that minimal Raman laser coupling is required (typically 10 to 50 times less than previous experiments using Raman coupling) thereby minimizing heating from spontaneous emission and enabling many-body experiments which require negligible heating rates. Lifetimes from spontaneous emission with this technique are in excess of 10 seconds, while all other approaches for creating large artificial gauge fields have lifetimes well below 1 second.

II.6 Topological Thouless pumping of ultracold fermions

Nakajima et al. [22] have built a Thouless pump using a flexible optical superlattice setup. This appears to be similar to the famous Archimedes screw, which pumps water via a rotating spiral tube. However, while the Archimedes screw follows classical physics and the pumped amount of water can be continuously changed by tilting the screw, the charge pumped by the Thouless pump is a topological quantum number and not affected by a smooth change of parameters. A gas of ultracold fermions atoms (Ytterbium atoms) have been prepared into dynamically controlled optical superlattice. This has been constructed through the interference of two laser beam creating two periodic potentials with different periods. The pumped charge depends only the trajectory generated by the periodic superlattice, as a consequence the charge is bound to winding number[6] in the plane of some parameters of system Hamiltonian. When the winding number assumes values different from zero the superlattice trajectory is topological, because the system has metallic edge states that permits the pumping of charge into superlattice. In the case of winding number zero the charge centre of mass is localized in initial position: the system is in a trivial phase.

[6] the winding number of a closed curve in the plane around a given point is an integer representing the total number of times that curve travels counter-clockwise around the point. The winding number depends on the orientation of the curve, and is negative if the curve travels around the point clockwise.

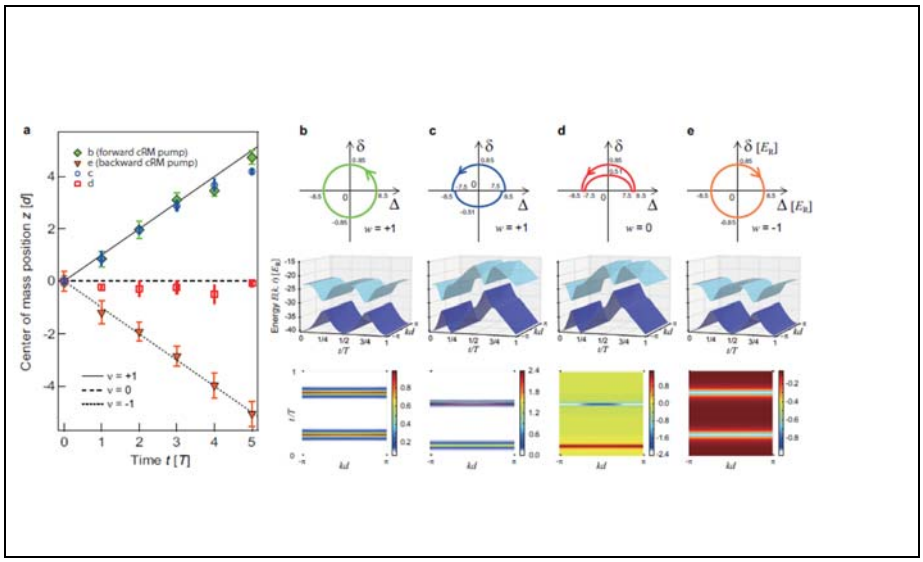

Figure -II.6- *(a) Behaviour of the centre of mass of pumped charge in function of time for different trajectories; (b), (c),(d), (e): energy gap of systems for different values of winding numbers* **.**

Chapter 3
RESULTS

III.1 Introduction

A core part of our investigation concerns the difference between standard order due to spontaneous symmetry breaking and topological order, and how to discriminate between the two addressing their different entanglement properties and patterns.

We have focused our attention on two 1-D models: the Ising spin-1/2 chain and the fermionic Kitaev chain with and without interaction. The Ising chain is a system formed by hard-core bosons realized through spin-flip operators acting on a Hilbert space with spin s = $\frac{1}{2}$. On the contrary, Kitaev chain is obtained replacing the bosonic spin operator of Ising chain with the spinless fermion creation and annihilation operators. We have found that both the states and the Hamiltonians are equivalent. The ground state of both models is two-fold degenerate, but the physics of the order displayed could hardly be more different. While in the Ising model the $\mathbb{Z}_2$ spin reflection symmetry is spontaneously broken, the degeneracy in the Kitaev chain stems from the Majorana zero mode (i.e., the isolated Majorana fermions at the ends of the chain that formed an entangled state of zero energy) characteristic of the topological order.

In order to determine rigorous criteria discriminating between the two types of order, in this chapter we thoroughly investigate an idea put forward by my PhD advisor, Prof. Fabrizio Illuminati, that a specific entanglement measure, the squashed entanglement that we have briefly introduced and described in Chapter I, is actually the natural order parameter for all those types of order, including topological phases of matter, that, at variance with Landau-Ginzburg types of order, emerge from a fine-grained division and interplay of different subsystems, thus depending naturally on multipartitions, state extensions, and state purifications. In particular, we will show how bipartite squashed entanglement for specific multipartitions is able to characterize and quantify the essential difference played by bulk and edge parts of symmetry-breaking and

topological chains. We will also report more recent results that we have obtained by applying this method to the investigation of other systems, including the one-dimensional cluster spin model and its symmetry-breaking counterparts, spin-1 chains with Heisenberg-like interactions, and higher-dimensional systems, such as the 2-D toric code model Hamiltonian.

III.2 A method to discriminate between spins with symmetry breaking order and Kitaev fermions with topological order

As we saw in the previous chapter, materials showing a topological order display a bulk band gap like an ordinary insulator, but a conducting surface state that is topologically protected by some symmetry. This implies looking for correlations not simply between two different halves of the same system, but between edges, and/or between edges and bulk, or even between different parts of the bulk. This in turn means introducing multipartitions instead of bipartitions. Therefore, in order to compare the different aspects of a topological (Kitaev) and non-topological (Ising) materials we begin by considering tripartitions and quadripartitions as in the following figure.

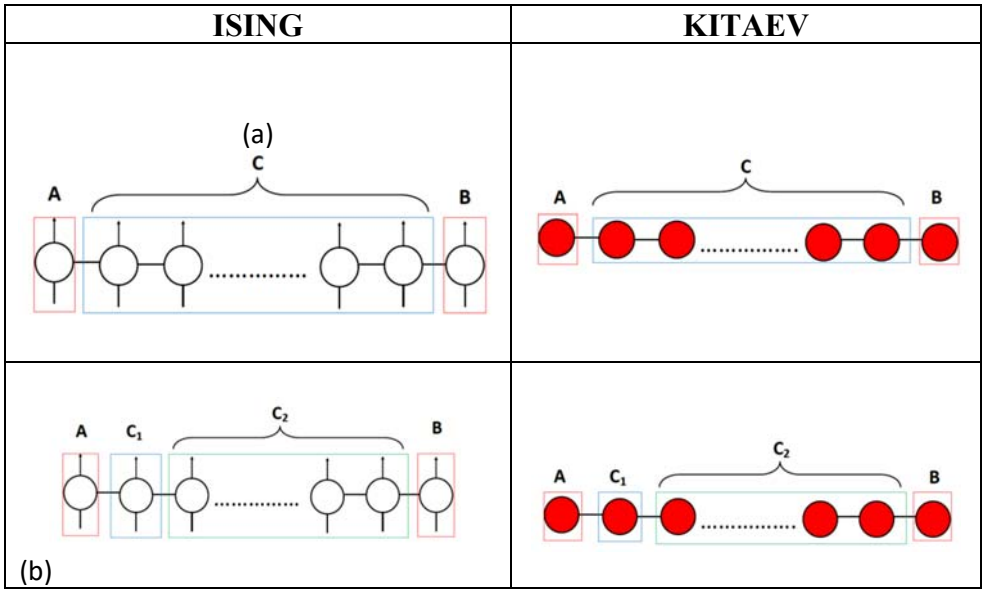

Figure III.1 *Examples of tripartitions (a) and quadripartitions (b) in Ising (left) and Kitaev (right) chains of finite size with open boundary conditions. A and B denote the two edges, while C denotes the bulk and* C_1 *and* C_2 *denote the two halves (not necessarily symmetric) of the same bulk C.*

Edge-bulk-edge tripartitions allow to investigate and characterize edge-edge and bulk-edge correlations, while edge-bulk-bulk-edge quadripartitions allow also to consider bulk-bulk correlations. Once multipartitions are introduced, more than one step of state reduction is necessary to characterize the states of the various subsystems, meaning that all bipartition-based measures of bipartite entanglement, such as, e.g., the von Neumann entanglement entropy, are bypassed as they cease to be meaningful entanglement quantifiers.

One thus needs a measure of bipartite entanglement that is nevertheless intrinsically based on state extension on multipartitions, and in particular on 4- and 3-partitions. In one of those rare shining moments in which concepts from a research field are integrally exported and applied to a seemingly very different one, such a bipartite entanglement measure naturally defined in terms of 4- and 3-partitions actually exists: indeed, it is the squashed entanglement. In terms of the latter, the *A*-*B* edge-edge long-distance entanglement $\mathcal{E}_{sq}^{ee}(\rho_{AB})$ in the reduced edge-edge, two-site state ρ_{AB} reads as follows:

- For a tripartition:

$$\mathcal{E}^{ee}_{sq,3}(\rho_{AB}) = \inf_{\rho_{ABC}} \{\frac{1}{2}(S(\rho_{AC}) + S(\rho_{BC}) - S(\rho_C) - S(\rho_{ABC})\};$$

(III.1)

- For a quadripartition:

$$\mathcal{E}^{ee}_{sq,4}(\rho_{AB}) = \inf_{\rho_{ABC_1}} \{\frac{1}{2}(S(\rho_{AC_1}) + S(\rho_{BC_1}) - S(\rho_{C_1}) - S(\rho_{ABC_1})\};$$

(III.1b)

Where ρ_{AB} is the reduced state of the edges *AB*, ρ_{ABC} is the ground state projector of the entire chain *ABC*.
$\rho_{ABC_1} = Tr_{C_2}(\rho_{ABC_1C_2})$ is the reduced state of the edges *AB* and the C_1 half of the bulk, $\rho_{ABC_1C_2}$ is the ground state projector of the entire chain ABC_1C_2, and *S* denotes the von Neumann entropy. One has to take the infimum in case of degenerate ground states and degenerate first reductions, otherwise the procedure is uniquely defined without extremization requirements. Now, if the system is topological the edge entanglement, that is the nonlocal edge-edge quantum correlations, must be independent of the bulk, irrespective of how it is partitioned. We thus expect the edge squashed entanglement to be insensitive and independent of the choice of the multipartition, either tripartition or quadripartition, in the case of the Kitaev chain. On the contrary, we expect that the edge squashed entanglement will depend on the way the bulk is partitioned when we consider symmetry breaking systems like the Ising chain. When the different parts of the systems become uncorrelated, as in disordered phases, these differences should disappear, implying that the squashed entanglement should behave as an order parameter. In the following paragraph we report the analytic findings that support our conjecture.

III.3 Non-interacting Kitaev chain: edge to edge squashed entanglement

As we need to compare the Ising and the Kitaev models, we begin by setting notations and expressions. The Hamiltonian for an Ising spin chain of finite size L in transverse field, with open boundary conditions, reads:

$$H_I = -\sum_{j=1}^{L-1} \sigma_j^x \sigma_{j+1}^x - h \sum_{j=1}^{L} \sigma_j^z , \qquad \text{(III. 2)}$$

Where L is the length of chain, h is the ration between the transverse magnetic field and the uniform spin-spin interaction strength, and σ_j^x and σ_j^z are, respectively, the x and z Pauli matrices. For $h = 0$, in the basis in which all the single-site matrices σ_j^x are diagonal, the two degenerate ground energy eigenstates read:

$$|\uparrow\uparrow\uparrow\cdots\uparrow\uparrow\rangle_x \qquad \text{and} \qquad |\downarrow\downarrow\downarrow\cdots\downarrow\downarrow\rangle_x \qquad \text{(III. 3)}$$

As symmetry-breaking and spontaneous magnetization cannot occur at zero field for a finite-size systems, we need to consider the physical states, namely the non-magnetic, i.e. zero-magnetization ground states that are also eigenstates of the Hamiltonian symmetry, i.e. the parity operator under spin flip. The physical ground space is formed by these states that coincide with the two L-particle GHZ maximally entangled states (also known as the L-particle entangled Schroedinger cat states) of definite parity (symmetry):

$$|\psi_{even}\rangle = \frac{1}{\sqrt{2}}[|\uparrow\uparrow\uparrow\cdots\uparrow\uparrow\rangle_x + |\downarrow\downarrow\downarrow\cdots\downarrow\downarrow\rangle_x];$$

$$|\psi_{odd}\rangle = \frac{1}{\sqrt{2}}[|\uparrow\uparrow\uparrow\cdots\uparrow\uparrow\rangle_x - |\downarrow\downarrow\downarrow\cdots\downarrow\downarrow\rangle_x]. \qquad \text{(III. 4)}$$

In terms of spin-flip operations the parity operator P reads:

$$P = \prod_{j=1}^{L} \sigma_j^z \qquad \text{(III. 5)}$$

It is immediate to verify that:

$$P|\psi_{even}\rangle = +|\psi_{even}\rangle\,;$$

$$P|\psi_{odd}\rangle = -|\psi_{even}\rangle\,. \qquad \text{(III. 6)}$$

Let us first consider the case $h = 0$. In order to compute the *A*-*B* edge to edge squashed entanglement $\mathcal{E}_{sq}$ of the reduced edge-edge state ρ_{AB} , we first write down the two ground state projectors in the tripartite case:

$$\rho_{ABC}^{even} = |\psi_{even}\rangle\langle\psi_{even}| = \frac{1}{2}[|\uparrow\uparrow\uparrow\cdots\uparrow\uparrow\rangle_x\langle\uparrow\uparrow\uparrow\cdots\uparrow\uparrow|_x + |\uparrow\uparrow\uparrow\cdots\uparrow\uparrow\rangle_x\langle\downarrow\downarrow\downarrow\cdots\downarrow\downarrow|_x + |\downarrow\downarrow\downarrow\cdots\downarrow\downarrow\rangle_x\langle\uparrow\uparrow\uparrow\cdots\uparrow\uparrow|_x + |\downarrow\downarrow\downarrow..\downarrow\rangle_x\langle\downarrow..\downarrow|_x];$$

$$\rho_{ABC}^{odd} = |\psi_{odd}\rangle\langle\psi_{odd}| = \frac{1}{2}[|\uparrow\uparrow\uparrow\cdots\uparrow\uparrow\rangle_x\langle\uparrow\uparrow\uparrow\cdots\uparrow\uparrow|_x - |\uparrow\uparrow\uparrow\cdots\uparrow\uparrow\rangle_x\langle\downarrow\downarrow\downarrow\cdots\downarrow\downarrow|_x - |\downarrow\downarrow\downarrow\cdots\downarrow\downarrow\rangle_x\langle\uparrow\cdots\uparrow\uparrow|_x + |\downarrow\cdots\downarrow\rangle_x\langle\downarrow..\downarrow|_x]\ . \qquad \text{(III. 8)}$$

It is immediate to verify that the final expressions are identical and do not depend on the degeneration, and thus coincide for both states. Therefore, in the following we can consider indifferently any of the two ground states. Here we need to pause and discuss in more detail the question of taking the *inf* in the definition of the squashed entanglement. Strictly speaking, taking the *inf* only with respect to the ground-state extensions of the reduced state ρ_{AB} does not guarantee that the ensuing expressions do coincide with the true squashed entanglement of ρ_{AB} rather than being simply an upper bound to it. On the other hand, we have numerically generated large sets of random purifications of ρ_{AB} and we have found no counterexample. Adding to this the recent discussion by the Bellomo group on the relationship between entanglement and energy, indicating that minimal energy and minimal entanglement bounds are strictly related, gives further strength to the conjecture that indeed the ground-state purification of ρ_{AB} realizes the *inf* and is thus associated to the true squashed edge entanglement. Needless to say, a definitive rigorous proof of this statement is still lacking and would be very welcome if this loophole could be closed in the near future. With this caveat, and choosing ρ_{ABC}^{even} among the two degenerate extensions of ρ_{AB} , we proceed to compute the different entropic terms entering the final expression of the edge-edge (possibly upper bound) squashed entanglement. From the definition:

$$\rho_{AC}^{even} = Tr_B(\rho_{ABC}^{even}) = \langle\uparrow_B |\rho_{ABC}^{even}| \uparrow_B\rangle + \langle\downarrow_B |\rho_{ABC}^{even}| \downarrow_B\rangle , \qquad \text{(III. 9)}$$

the reduced state ρ_{AC}^{even} reads

$$\rho_{AC}^{even} = \frac{1}{2}[|\uparrow\uparrow\uparrow\cdots\uparrow\rangle_x\langle\uparrow\uparrow\cdots\uparrow\uparrow|_x + |\downarrow\downarrow\cdots\downarrow\downarrow\rangle_x\langle\downarrow\downarrow\cdots|_x] \ , \ \text{(III. 10)}$$

and the corresponding von Neumann entropy reads:

$$S(\rho_{AC}^{even}) = -\frac{1}{2}\ln\left(\frac{1}{2}\right) - \frac{1}{2}\ln\left(\frac{1}{2}\right) = \ln(2) \ . \qquad \text{(III. 11)}$$

The computation of the other reduced entropies is analogous and we obtain:

$$S(\rho_{AC}^{even}) = S(\rho_{BC}^{even}) = S(\rho_{C}^{even}) = \ln(2) \ , \qquad \text{(III. 11bis)}$$

while of course for the pure ground state projector ρ_{ABC}^{even} we have:

$$S(\rho_{ABC}^{even}) = 0 \ . \qquad \text{(III. 12)}$$

Therefore, the end-to-end (edge-edge) squashed entanglement of the two-edge reduced state ρ_{AB} in the case of a 3-partition reads:

$$\mathcal{E}_{sq,3}^{ee}(\rho_{AB}) = \frac{\ln(2)}{2} \ . \qquad \text{(III. 13)}$$

We can repeat the same procedure in the case of the edge-bulk-bulk-edge AC_1C_2B quadripartition. As the result is independent of the choice of the ground state, considering again the even state, we have:

$$\begin{aligned}\rho_{AC_1C_2B}^{even} = \frac{1}{2}[&|\uparrow\uparrow\uparrow\cdots\uparrow\uparrow\rangle_x\langle\uparrow\uparrow\uparrow\cdots\uparrow\uparrow|_x + |\uparrow\uparrow\uparrow\cdots\uparrow\uparrow\rangle_x\langle\downarrow\downarrow\downarrow\cdots\downarrow\downarrow|_x \\ &+ |\downarrow\downarrow\downarrow\cdots\downarrow\downarrow\rangle_x\langle\uparrow\uparrow\uparrow\cdots\uparrow\uparrow|_x \\ &+ |\downarrow\downarrow\downarrow\cdots\downarrow\downarrow\rangle_x\langle\downarrow\downarrow\downarrow\cdots\downarrow\downarrow|_x] \ . \qquad \text{(III. 14)}\end{aligned}$$

Next, we determine the reduced density matrices. Remarkably, one can verify that the symmetry of the bulk partitioning is irrelevant and that the final result does not depend on it. This feature allows for a very handy simplification, as it will suffice to take the first half C_1 of the bulk made by just one spin, and the second half C_2 made of the remaining L – 3 total bulk spins, so that we can always work, without loss of generality, with 3-spin, 2-spin, and 1-spin reduced states as follows:

$$\rho_{ABC_1}^{even} = \frac{1}{2}[|\uparrow\uparrow\uparrow\rangle_x\langle\uparrow\uparrow\uparrow|_x + |\downarrow\downarrow\downarrow\rangle_x\langle\downarrow\downarrow\downarrow|_x];$$

$$\rho_{AC_1}^{even} = \rho_{BC_1}^{even} = \frac{1}{2}[|\uparrow\uparrow\rangle_x\langle\uparrow\uparrow|_x + |\downarrow\downarrow\rangle_x\langle\downarrow\downarrow|_x]; \qquad \text{(III. 15)}$$

$$\rho_{C_1}^{even} = \frac{1}{2}[|\uparrow\rangle_x\langle\uparrow|_x + |\downarrow\rangle_x\langle\downarrow|_x]. \qquad \text{(III. 16)}$$

Computing the corresponding entropies and collecting results, we have that edge-edge squashed entanglement of the two-edge reduced state ρ_{AB} in the case of a 4-partition is:

$$\mathcal{E}_{sq,4}^{ee}(\rho_{AB}) = 0. \qquad \text{(III. 17)}$$

Comparing (III.13) and (III.17) we see that indeed in the case of the Ising chain the end to end edge-edge squashed entanglement takes completely different values in correspondence of a structured vs an undivided bulk.

We now move to consider the case of the non-interacting Kitaev fermionic chain of finite size L, with open boundary conditions, whose model Hamiltonian reads:

$$H_K = \sum_{j=1}^{L-1}\left[-t\left(c_j^+ c_{j+1} + c_{j+1}^+ c_j\right) + \Delta\left(c_j c_{j+1} + c_{j+1}^+ c_j^+\right)\right]$$

$$-\frac{1}{2}\sum_{j=1}^{L}\mu\left(2c_j^+ c_j - 1\right). \qquad \text{(III. 18)}$$

Here t is the coefficient of the hopping term, Δ is the coefficient of the pairing term, and μ denotes the chemical potential. The operators c_j^+ and c_j are respectively the creation and annihilation operators. We consider the case $\Delta = t$, for which we are assured to be in a topological phase as long as $\mu \leq 2$. To fix the formalism, let us consider the simples instance L=4 of a chain with two minimal bulk halves. Using the Jordan-Wigner transformation [23] we have the following ground-space:

$$|\psi_{even}\rangle = \frac{1}{2\sqrt{2}}[|1111\rangle + |1001\rangle + |0101\rangle + |1100\rangle + |0110\rangle +$$

$$|0011\rangle + |0000\rangle + |1010\rangle]; \qquad \text{(III. 19)}$$

$$|\psi_{odd}\rangle = \frac{1}{2\sqrt{2}}[|1110\rangle + |1101\rangle + |0111\rangle + |0100\rangle + |1011\rangle$$

$$+ |1000\rangle + |0010\rangle + |0001\rangle]; \qquad \text{(III. 20)}$$

where the state $|1\rangle$ corresponds to a site occupied by one fermion and an empty site corresponds to state $|0\rangle$. The Kitaev chain Hamiltonian is invariant under parity symmetry operations realized by the following parity operator:

$$P = \prod_{j=1}^{L}\left(1 - c_j^+ c_j\right). \qquad \text{(III. 21)}$$

To implement the algorithm for the squashed entanglement at $\mu = 0$ one can resort to the Peschel reduced density matrix method for free fermions [29], that we describe in detail in appendix A. Using such exact technique, we find that the squashed entanglement coincides for both partitions:

$$\mathcal{E}^{ee}_{sq,3}(\rho_{AB}) = \mathcal{E}^{ee}_{sq,4}(\rho_{AB}) = \frac{\ln 2}{2}\,. \qquad \text{(III. 22)}$$

Moving on to consider the entire range of values of *h* for the Ising model and of μ for the non-interacting Kitaev chain, we have resorted to exact diagonalization, developing a specific Mathematica package optimizing the computational routine. We were thus able to solve for chains up to L = 14 sites. The results are reported in Figure III.2 below.

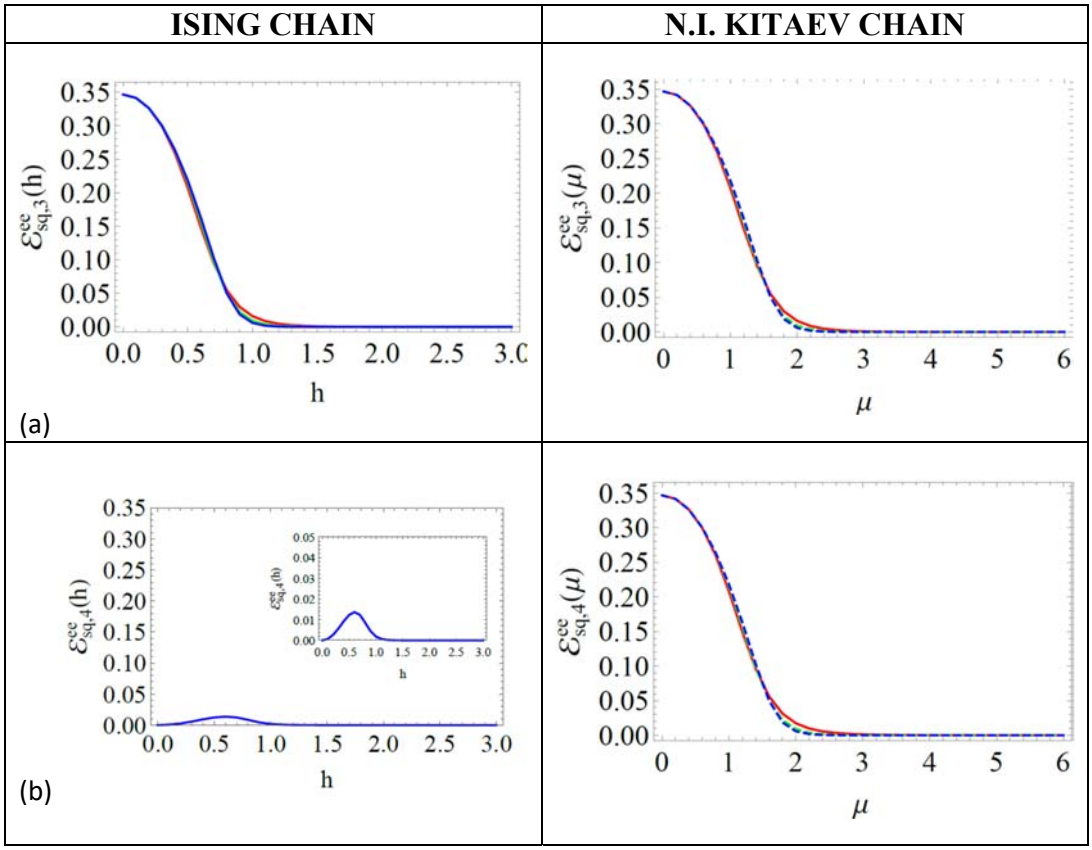

Figure III.2 *Behaviour of the bipartite edge-edge squashed entanglement* $\mathcal{E}_{sq}^{ee}(\rho_{AB})$ *of the two-edge state* ρ_{AB} *for the open Ising chain as a function of the external field h and for the open non-interacting Kitaev chain as a function of the chemical potential μ. Panels (a), from left to right: Ising and Kitaev edge-edge squashed entanglement for the (ACB) tripartition edge-bulk-edge and different chain lengths (L = 10, 12, 14). Panels (b), from left to right: Ising and Kitaev edge-edge squashed entanglement for the* (AC_1C_2B) *quadripartition edge-bulk-bulk-edge and different chain lengths (Ising: L = 14; Kitaev: L = 10, 12, 14). Red lines: L = 10; green lines: L = 12; blue lines: L = 14.*

We see that the squashed entanglement:

- Identifies the phase transition for the Ising and the non-interacting Kitaev chain;
- It is bulk-independent for the non-interacting Kitaev chain.

Indeed, correlations do spread locally in a symmetry-breaking environment. As a consequence, the quantum entanglement at the boundaries must depend on how the bulk is manipulated. On the contrary, the entanglement between the edges in a topological environment must be decoupled from the bulk and how it is divided, traced, and manipulated. By its very definition, the squashed entanglement is the ideal quantity able to discriminate between these two different physical-geometric classes of environments, as we will show in the following. The results illustrated in this chapter have been obtained by me with the support of my PhD advisor Prof. F. Illuminati, and build on his ideas about the role of squashed entanglement in the study of quantum matter, which in turn were motivated by pioneering intuitions on multipartitions and entropic invariants put forwards by X.-G. Wen and collaborators in the book "*Quantum Information Meets Quantum Matter*" by Bei Zeng, Xie Chen, Duan-Lu Zhou, and Xiao-Gang Wen (Springer, NY, 2019), and by M. Dalmonte and collaborators in the paper "*Entanglement topological invariants for one-dimensional topological superconductors*" by P. Fromholz, G. Magnifico, V. Vitale, T. Mendes-Santos, and M. Dalmonte, Physical Review B **101**, 085136 (2020).

III.4 Edge to bulk and bulk to bulk squashed entanglement

The results that we have obtained in the previous subsection highlight the different bulk proprieties of the Ising and Kitaev chains. The crucial understanding that the Kitaev chain bulk is insulating and the Ising chain one is conductive explains the different behaviours of the edge-edge squashed entanglement in the two model systems. From this fundamental physical observation, we can immediately deduce a second method to discriminate between the two chains by considering the entanglement between the edge and the bulk degrees of freedom. In the following figure we report the edge-bulk squashed entanglement; we see that it is zero for the Kitaev chain (to be precise, it vanishes exponentially with increasing chain size) and different from zero (in the ordered phase) for the Ising chain.

ISING CHAIN	N.I. KITAEV CHAIN
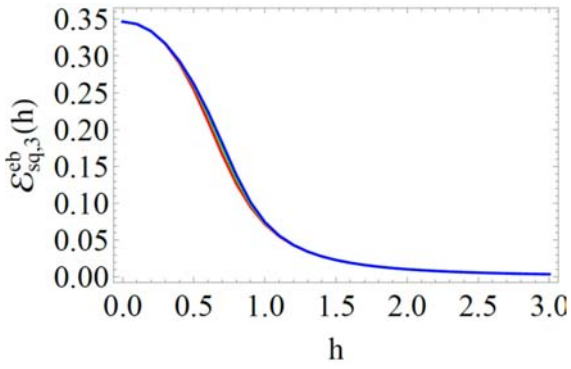	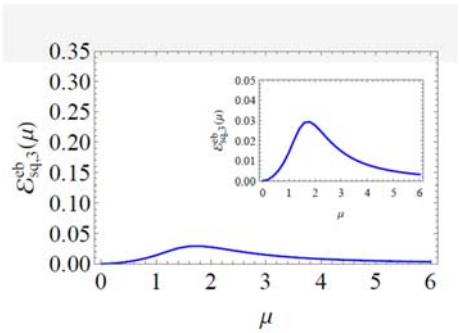

Figure III.3 *Behaviour of the bipartite edge-bulk squashed entanglement* $\mathcal{E}^{eb}_{sq,3}(\rho_{AC}) = \mathcal{E}^{eb}_{sq,3}(\rho_{BC})$ *for the open Ising chain (L = 8,10,12) and the open non-interacting Kitaev chain (L = 8) for the (ACB) tripartition edge-bulk-edge. The results have been obtained by exact numerical diagonalization using an optimized Mathematica package.*

We see that, contrary to the edge-edge instance, comparing the edge-bulk squashed entanglements at the tripartition level is sufficient to discriminate between the Ising and the non-interacting Kitaev chains. As the bulk does not diffuse information in the topological phase, its correlation with the edges vanishes exponentially in the system size. From there on, the edges and the bulk remain decoupled irrespective of any further manipulation, tracing, modification of the bulk and the results are thus invariant with respect to the choice of the multipartition. Remarkably, investigating the bulk-bulk squashed entanglement and comparing between the two chains yields the same results. In summary, looking at the squashed entanglement between the edges discriminates at the quadripartition level, as local modifications of the bulk environment (like tracing away only one part of the bulk instead of the entire bulk) affect the boundary degrees of freedom of locally ordered systems but not the edge states of globally (topologically) ordered systems. On the other hand, looking at the edge-bulk squashed entanglement discriminates already at the tripartite level, as bulk and boundary degrees of freedom are correlated in a symmetry-breaking system and exponentially decoupled in a topological system.

In the following, we illustrate the reasons underlying the different bulk behaviours for two chains, highlighting the role of the Majorana fermions in the Kitaev Hamiltonian. The Kitaev chain belongs to the set of symmetry-protected one-dimensional topological systems. They share the feature of having physical

edges with degenerate ground states. In particular, for $t = \Delta$ and $\mu = 0$, we have:

$$H_K = it\sum_{n=1}^{L-1}\gamma_{2n}\gamma_{2n+1}\,; \qquad \text{(III. 23)}$$

where i is the imaginary unit, t is the hopping term, L is the length of chain and:

$$\gamma_{2n} = -i(c_n - c_n^+);$$

$$\gamma_{2n-1} = (c_n + c_n^+). \qquad \text{(III. 24)}$$

We can see that the two Majorana modes γ_1 and γ_{2L} at the edges do not enter at all in H_K. Hence our chain has two zero-energy states, localized at its ends. All the states which are not at the ends of the chain have an energy of $\pm|t|$. The zero-energy oscillation of the edges generates a quantum correlation between the edges independent of the bulk. Furthermore, this correlation is protected by the fermionic parity which acts on the edges in an anomalous way. Let us consider the following example for a chain of length L=4; for μ=0 the even ground state of the Kitaev chain reads:

$$|\psi_{even}\rangle = \frac{1}{2\sqrt{2}}[|1111\rangle + |1001\rangle + |0101\rangle + |1100\rangle + |0110\rangle + |0011\rangle + |0000\rangle + |1010\rangle]. \qquad \text{(III. 25)}$$

The fermionic parity operator can be written in terms of the Majorana fermionic operators as follows:

$$P = \prod_n i\gamma_{2n}\gamma_{2n+1}\,. \qquad \text{(III. 26)}$$

It is straightforward to check that the operator defined as: $P' = i\gamma_{2L}\gamma_1 = P_R P_L$, acts on $|\psi_{even}\rangle$ as the operator P. This happens also for the operator $P' = -P_R P_L$. The existence of two operators that commute with Hamiltonian operator and act on a state only for the left and right edges explains the nature of two edges modes as the present example illustrates. For the even ground

states of a L=4 chain at $\mu = 0$ the zero edge modes are γ_1 and γ_8 . From eq. (III.26) we have:

$$P' = i\gamma_8\gamma_1 = c_4c_1 + c_4c_1^+ - c_4^+c_1 - c_4^+c_1^+. \qquad \text{(III. 27)}$$

It is immediate to verify that applying the operator P to the even ground state yields

$$P_RP_L|1111\rangle \rightarrow |0110\rangle;$$

$$P_RP_L|0110\rangle \rightarrow |1111\rangle;$$

$$P_RP_L|0000\rangle \rightarrow |1001\rangle;$$

$$P_RP_L|1001\rangle \rightarrow |0000\rangle;$$

$$P_RP_L|0101\rangle \rightarrow |1100\rangle \qquad \text{(III. 28)}$$

and so on.

The application of the operator P_RP_L recomposes the even ground-states in the Kitaev chain. This is not true for the Ising chain. Indeed, the parity operator for the Ising Hamiltonian is defined as:

$$\prod_j \sigma_j^z. \qquad \text{(III. 29)}$$

In the Ising case there do not exist two left and right parity operators like in the case of the Kitaev chain. This implies that the correlations between the two Ising edges are mediated by spin bulk correlations.

III.5 Diamagnetic edges

We can say that for the non-interacting Kitaev chain the Majorana edge fermions go into gapless energy states due to their non-Abelian statistics. They oscillate in different directions producing in this way a quantum correlation. All the other bulk fermions are not correlated with the edges because they are in excited states and preserve their fermionic nature. The increment in the on-site energy leads to a reduction in the scattering between the two edges due to the opening of a gap and the Majorana edge fermions become uncorrelated with the bulk.

For the Ising chain a similar phenomenon occurs but with a substantial difference due to the spin correlations of the particles. The two edge spins go into a gapless state with lower energy, but the other spins remain correlated with the edges to minimize the energy of the entire system.

In order to verify these assertions, we should investigate the consequences of dynamically locating the two edge spins in the gapless energy states. This can be done by introducing a local disorder in such a way that the two edge spins are effectively coupled to a smaller magnetic field with respect to the bulk sites.

We have assumed throughout that the entanglement between the two edges of the chain is maximal when the edges are in the ground state for $h = 0$ (Ising chain) or $\mu = 0$ (Kitaev chain). As h or μ increase, the edges increase their energy and this should favour a reduction of the entanglement.

If we wish to stabilize the end to end entanglement between the edges, they must remain localized in the ground state throughout the ordered phase. In order to achieve this objective, we can provide the two edges with suitable diamagnetic properties that result in them being acted upon by an effective external magnetic field that is weaker than the actual field acting on the bulk. By a diamagnetic edge we thus mean a quantum degree of freedom that is affected by a reduced magnetic field or chemical potential.

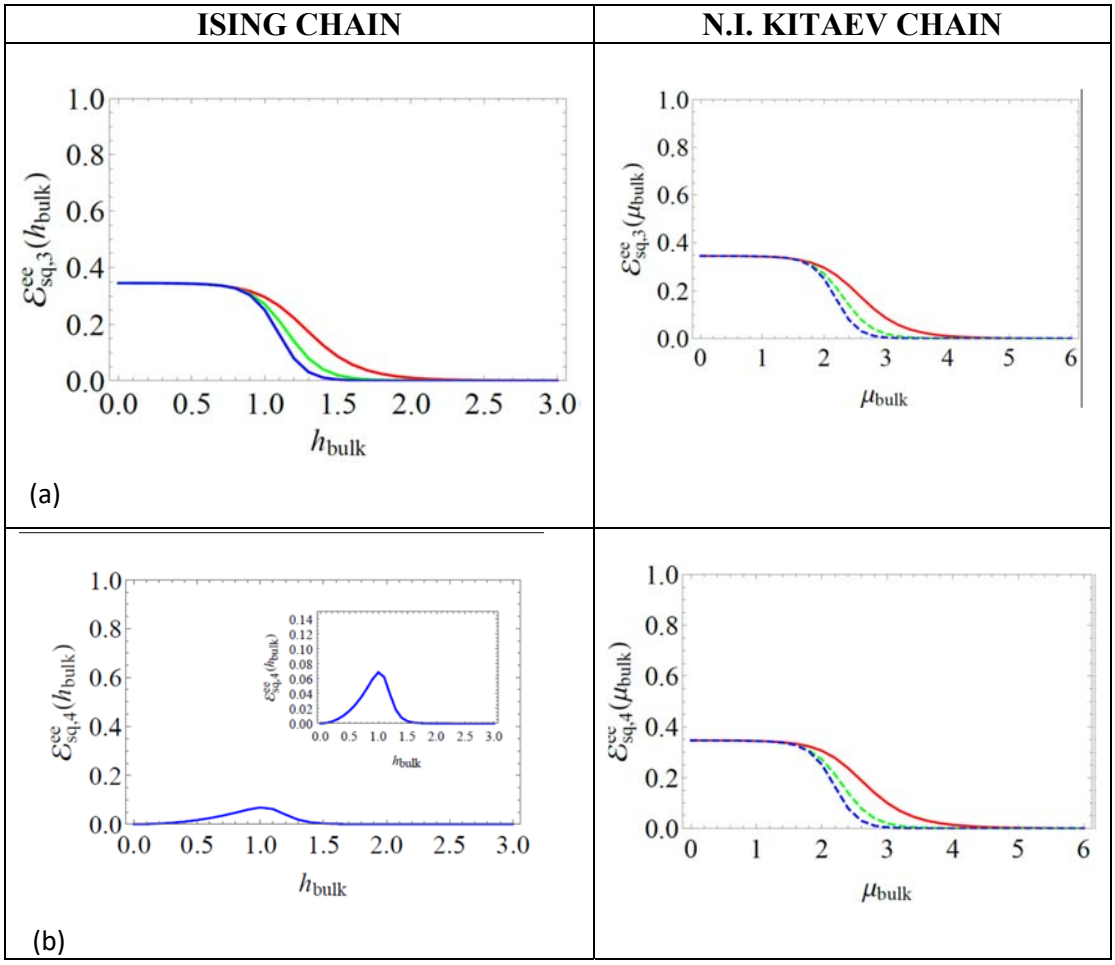

Figure III.4 *Behaviour of the edge-edge bipartite squashed entanglement in the Ising and in the non-interacting Kitaev open chains for: (a) the tripartition edge-bulk-edge (ACB) and chain size L = 10,12,14 for both models; and for: (b) the quadripartition edge-bulk-bulk-edge (AC_1C_2B) and chain size L = 14 for the Ising system and L = 10, 12, 14 for the Kitaev system. Red line: L = 10; green line: L = 12; blue line: L = 14. The results have been obtained numerically using Mathematica package.*

In Fig. (III.4) panel (a) we report the behaviour of the squashed edge-edge entanglement for a tripartition of the Ising chain where the edges are affected by an external magnetic field $\boldsymbol{h_{edge} = \frac{h_{bulk}}{10}}$. Entanglement is effectively stabilized throughout the ordered phase. This stabilization depends on the fact that the edges are dynamically located in the ground state. The same result is

obtained for a Kitaev chain with $\boldsymbol{\mu_{edge}} = \frac{\boldsymbol{\mu_{bulk}}}{\mathbf{5}}$. The situation is completely different if one considers a quadripartition. In this case, as shown in Fig. (III.4) panel (b), the edge-edge entanglement discriminates unambiguously between the Ising and the non-interacting Kitaev chain.

Indeed, the bulk and the edges have different properties in both models, and these differences are again captured by a sufficiently accurate multipartition of the systems. In particular, the bulk is located in an energy level separated by a gap with respect to the energy level of the two edges. In other words, the interaction between the particles in the two chains generates quasi-particles localized at the edges which have a lower energy than the bulk. These quasi-particles have a different nature. In the Kitaev chain (composed of spinless fermions) we have Majorana fermions, while for the Ising chain (composed of spin-1/2 degrees of freedom) the correlations between the spins generate the magnons (spin waves). Each Majorana fermion of the bulk is correlated only with its first neighbour, which determines an insulating bulk, while magnons have a global correlation along the entire chain, manifesting a conductive bulk.

III.5 Diamagnetic edges and ground state fidelity: robustness against local perturbations

An additional route to investigate the role of diamagnetic edges and verify the previous entanglement-based discrimination by an independent method is provided by resorting to the ground state fidelity. Fidelity is a measure of how "close" ("similar") are two quantum states. It expresses the probability that one state will pass a test to identify as the other. Given two states represented by two density operators ρ_1 and ρ_2, the Uhlmann fidelity is defined as:

$$\mathcal{F}(\rho_1, \rho_2) = Tr\sqrt{\sqrt{\rho_1}\rho_2\sqrt{\rho_1}}. \qquad (III.30)$$

We consider the ground-state of edge partition for $h/\mu = 0$ (i.e. $\rho_1(h/\mu = 0)$) and for $h/\mu \neq 0$ (i.e. $\rho_2(h/\mu \neq 0)$) and we have determined the Fidelity between $\rho_1(h/\mu = 0)$ and $\rho_2(h/\mu \neq 0)$ in case of "normal edges" and in the case of "diamagnetic edges".

ISING CHAIN	KITAEV CHAIN
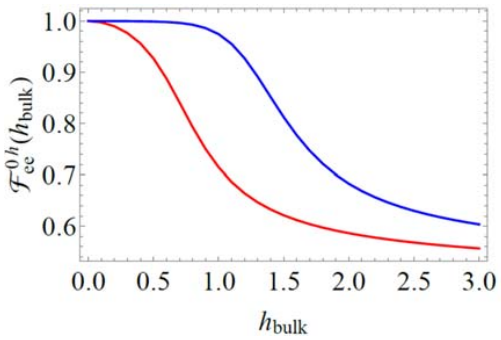	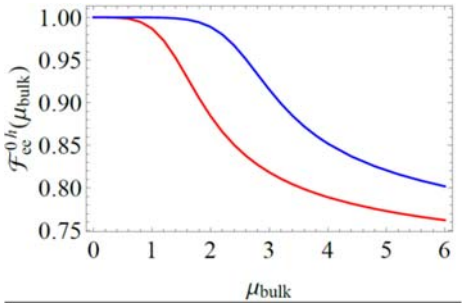

Figure III.5 *Comparison of Fidelity for the Ising chain and the non-interacting Kitaev chain for L = 10. Red curve: normal edges, blue curve: diamagnetic edges. The results have been obtained numerically with Mathematica package.*

We observe that both in the Ising and non-interacting Kitaev chains the fidelity assumes its maximal value in the case of diamagnetic edges. This means that the edges are located in the same ground state respectively in the ordered magnetic phase (Ising chain) as well as in the topological phase (Kitaev chain). From this point of view, a bipartite quantity like the fidelity does not discriminate qualitatively between the two types of order, as expected. On the other hand, we observe that the fidelity in the Kitaev chain assumes values that are always larger than the fidelity in the Ising chain for the corresponding values of the Hamiltonian parameters, and maximally so in the topological phase. This fact provides further evidence that topological systems are more resilient with respect to local perturbations such as the local, on-site variations of the chemical potential.

III.6 The role of interactions: Comparing *XYZ* spin chains and interacting Kitaev chains

In this section we extend the previous results to the fully interacting case. Let us thus consider first the *XYZ* spin chain that corresponds, via the Jordan-Wigner transformation, to an interacting Kitaev fermionic chain. For a chain of finite size L and open boundary conditions, the two models are described, respectively, by the Hamiltonians:

$$H_{XYZ} = \sum_{j=1}^{L-1} -J_x \sigma_j^x \sigma_{j+1}^x - J_y \sigma_j^y \sigma_{j+1}^y + J_z \sigma_j^z \sigma_{j+1}^z \; - \sum_{j=1}^{L} h_f \sigma_j^z \; ; \qquad \text{(III. 31)}$$

$$H_{KI} = \sum_{j=1}^{2L-1} \left[-t\left(c_j^+ c_{j+1} + c_{j+1}^+ c_j\right) + \Delta\left(c_j c_{j+1} + c_{j+1}^+ c_j^+\right) \right] - \frac{1}{2} \sum_{j=1}^{2L} \mu\left(2c_j^+ c_j - 1\right) + U \sum_{j=1}^{L-1} (2c_j^+ c_j - 1)(\, 2c_j^+ c_j + 1) \, . \qquad \text{(III. 32)}$$

For the *XYZ* chain it is possible to obtain explicit exact solutions along the factorization line that corresponds to the following values of the external field:

$$h_f = \sqrt{(J_x + J_z)(J_y + J_z)} \; ; \qquad \text{(III. 33)}$$

h_f is the factorizing field: for these values of the external magnetic field the two-fold degenerate ground states are factorized, i.e. they are unentangled, product states of single-site quantum wave functions [26]:

$$|\psi_1\rangle = \frac{1}{(1+\alpha^2)^{\frac{L}{2}}} \otimes_{j=1}^{L} \left(|\uparrow\rangle_j + \alpha |\downarrow\rangle_j \right);$$

$$|\psi_2\rangle = \frac{1}{(1+\alpha^2)^{\frac{L}{2}}} \otimes_{j=1}^{L} \left(|\uparrow\rangle_j + \alpha |\downarrow\rangle_j \right); \qquad \text{(III. 34)}$$

where $\alpha = \sqrt{\cot\left(\frac{arctang\left(\frac{J_x - J_y}{h_f}\right)}{2} \right)}$.

The physical ground states are of course the entangled linear combinations that satisfy the parity symmetry of all finite-size systems (the entangled "cats"):

$$|\psi_{even}\rangle = \frac{1}{\sqrt{2}}(|\psi_1\rangle + |\psi_2\rangle);$$

$$|\psi_{odd}\rangle = \frac{1}{\sqrt{2}}(|\psi_1\rangle - |\psi_2\rangle). \qquad \text{(III. 35)}$$

Starting from an interacting Kitaev model Hamiltonian we have the following mapping to the interacting XYZ spin Hamiltonian:

$$J_x = \frac{t+\Delta}{2}; \qquad J_y = \frac{t-\Delta}{2}; \qquad h_f = -\frac{\mu_f}{2};$$

where (See, e.g., Ref. [26]):

$$\mu_f = 2\sqrt{U^2 + tU + (t^2 - \Delta^2)/4} \quad . \qquad \text{(III. 36)}$$

The corresponding factorized ground states for the interacting Kitaev chain read:

$$|\psi_1\rangle = \frac{1}{(1+\alpha^2)^{\frac{L}{2}}} \bigotimes_{j=1}^{L} \left(e^{\alpha c_j^+}\right)|0\rangle\,;$$

$$|\psi_2\rangle = \frac{1}{(1+\alpha^2)^{\frac{L}{2}}} \bigotimes_{j=1}^{L} \left(e^{-\alpha c_j^+}\right)|0\rangle\,. \qquad \text{(III. 37)}$$

The states (III.37) are orthonormal and form the physical ground-space of the interacting Kitaev Hamiltonian.

In the following we illustrate in detail the analytic algorithm to determine the squashed entanglement for the XYZ and the interacting Kitaev chains in the simplest case L = 4, both for a tripartition and a quadripartition of the two models.

XYZ chain

For the XYZ chain consider the even state:

$$|\psi_{even}\rangle = \frac{1}{\sqrt{1+6\alpha^4+\alpha^8}}[|\uparrow\uparrow\uparrow\uparrow\rangle + \alpha^2|\uparrow\downarrow\downarrow\uparrow\rangle + \alpha^2|\downarrow\uparrow\uparrow\downarrow\rangle + \alpha^4|\downarrow\downarrow\downarrow\downarrow\rangle + \alpha^2|\uparrow\downarrow\uparrow\downarrow\rangle + \alpha^2|\uparrow\uparrow\downarrow\downarrow\rangle + \alpha^2|\downarrow\downarrow\uparrow\uparrow\rangle + \alpha^2|\downarrow\uparrow\downarrow\uparrow\rangle] \quad \text{(III. 38)}$$

In the case of an edge-bulk-edge *(ACB)* tripartition we obtain the following reduced density matrices:

$$\rho_{AC} = \rho_{CB} = \frac{1}{1+6\alpha^4+\alpha^8}\begin{pmatrix} 1 & 0 & 0 & 0 & \alpha^2 & \alpha^2 & \alpha^2 & 0 \\ 0 & \alpha^4 & \alpha^4 & \alpha^4 & 0 & 0 & 0 & \alpha^6 \\ 0 & \alpha^4 & \alpha^4 & \alpha^4 & 0 & 0 & 0 & \alpha^6 \\ 0 & \alpha^4 & \alpha^4 & \alpha^4 & 0 & 0 & 0 & \alpha^6 \\ \alpha^2 & 0 & 0 & 0 & \alpha^4 & \alpha^4 & \alpha^4 & 0 \\ \alpha^2 & 0 & 0 & 0 & \alpha^4 & \alpha^4 & \alpha^4 & 0 \\ \alpha^2 & 0 & 0 & 0 & \alpha^4 & \alpha^4 & \alpha^4 & 0 \\ 0 & \alpha^6 & \alpha^6 & \alpha^6 & 0 & 0 & 0 & \alpha^8 \end{pmatrix}$$

and

$$\rho_C = \frac{1}{1+6\alpha^4+\alpha^8}\begin{pmatrix} 1+\alpha^4 & 0 & 0 & \alpha^2+\alpha^6 \\ 0 & 2\alpha^4 & 2\alpha^4 & \\ 0 & 2\alpha^4 & 2\alpha^4 & \\ \alpha^6+\alpha^2 & 0 & 0 & \alpha^8+\alpha^4 \end{pmatrix}.$$

(III.39)

In the case of the odd ground state:

$$|\psi_{odd}\rangle = \frac{1}{2\sqrt{\alpha^2+\alpha^6}}[\alpha|\downarrow\uparrow\uparrow\uparrow\rangle + \alpha|\uparrow\downarrow\uparrow\uparrow\rangle + \alpha|\uparrow\uparrow\downarrow\uparrow\rangle + \alpha|\uparrow\uparrow\uparrow\downarrow\rangle + \alpha^3|\uparrow\downarrow\downarrow\downarrow\rangle + \alpha^3|\downarrow\uparrow\downarrow\downarrow\rangle + \alpha^3|\downarrow\downarrow\uparrow\downarrow\rangle + \alpha^3|\downarrow\downarrow\downarrow\uparrow\rangle], \quad \text{(III. 40)}$$

the reduced density matrices are:

$$\rho_{AC} = \rho_{CB} = \frac{1}{4\alpha^2+4\alpha^6}\begin{pmatrix} \alpha^2 & 0 & 0 & 0 & \alpha^4 & \alpha^4 & \alpha^4 & 0 \\ 0 & \alpha^2 & \alpha^2 & \alpha^2 & 0 & 0 & 0 & \alpha^4 \\ 0 & \alpha^2 & \alpha^2 & \alpha^2 & 0 & 0 & 0 & \alpha^4 \\ 0 & \alpha^2 & \alpha^2 & \alpha^2 & 0 & 0 & 0 & \alpha^4 \\ \alpha^4 & 0 & 0 & 0 & \alpha^6 & \alpha^6 & \alpha^6 & 0 \\ \alpha^4 & 0 & 0 & 0 & \alpha^6 & \alpha^6 & \alpha^6 & 0 \\ \alpha^4 & 0 & 0 & 0 & \alpha^6 & \alpha^6 & \alpha^6 & 0 \\ 0 & \alpha^4 & \alpha^4 & \alpha^4 & 0 & 0 & 0 & \alpha^6 \end{pmatrix}$$

and

$$\rho_C = \frac{1}{4\alpha^2+4\alpha^6}\begin{pmatrix} 2\alpha^2 & 0 & 0 & 2\alpha^4 \\ 0 & \alpha^2+\alpha^6 & \alpha^2+\alpha^6 & 0 \\ 0 & \alpha^2+\alpha^6 & \alpha^2+\alpha^6 & 0 \\ 2\alpha^4 & 0 & 0 & 2\alpha^6 \end{pmatrix}.$$

(III.41)

Next, we consider an edge-bulk-bulk-edge (AC_1C_2B) quadripartition and we perform the partial traces over the even ground state, obtaining:

$$\rho_{AC_1B} = \frac{1}{1+6\alpha^4+\alpha^8}\begin{pmatrix} 1 & 0 & 0 & 0 & \alpha^2 & \alpha^2 & \alpha^2 & 0 \\ 0 & \alpha^4 & \alpha^4 & \alpha^4 & 0 & 0 & 0 & \alpha^6 \\ 0 & \alpha^4 & \alpha^4 & \alpha^4 & 0 & 0 & 0 & \alpha^6 \\ 0 & \alpha^4 & \alpha^4 & \alpha^4 & 0 & 0 & 0 & \alpha^6 \\ \alpha^2 & 0 & 0 & 0 & \alpha^4 & \alpha^4 & \alpha^4 & 0 \\ \alpha^2 & 0 & 0 & 0 & \alpha^4 & \alpha^4 & \alpha^4 & 0 \\ \alpha^2 & 0 & 0 & 0 & \alpha^4 & \alpha^4 & \alpha^4 & 0 \\ 0 & \alpha^6 & \alpha^6 & \alpha^6 & 0 & 0 & 0 & \alpha^8 \end{pmatrix},$$

$$\rho_{AC_1} = \rho_{C_1B} = \frac{1}{1+6\alpha^4+\alpha^8}\begin{pmatrix} 1+\alpha^4 & 0 & 0 & \alpha^2+\alpha^6 \\ 0 & 2\alpha^4 & 2\alpha^4 & \\ 0 & 2\alpha^4 & 2\alpha^4 & \\ \alpha^6+\alpha^2 & 0 & 0 & \alpha^8+\alpha^4 \end{pmatrix}.$$

and

$$\rho_{C_1} = \frac{1}{1+6\alpha^4+\alpha^8}\begin{pmatrix} 1+3\alpha^4 & 0 \\ 0 & 3\alpha^4+\alpha^8 \end{pmatrix}.$$

(III.42)

For the odd ground state we obtain:

$$\rho_{AC_1B} = \frac{1}{4\alpha^2+4\alpha^6}\begin{pmatrix} \alpha^2 & 0 & 0 & 0 & \alpha^4 & \alpha^4 & \alpha^4 & 0 \\ 0 & \alpha^2 & \alpha^2 & \alpha^2 & 0 & 0 & 0 & \alpha^4 \\ 0 & \alpha^2 & \alpha^2 & \alpha^2 & 0 & 0 & 0 & \alpha^4 \\ 0 & \alpha^2 & \alpha^2 & \alpha^2 & 0 & 0 & 0 & \alpha^4 \\ \alpha^4 & 0 & 0 & 0 & \alpha^6 & \alpha^6 & \alpha^6 & 0 \\ \alpha^4 & 0 & 0 & 0 & \alpha^6 & \alpha^6 & \alpha^6 & 0 \\ \alpha^4 & 0 & 0 & 0 & \alpha^6 & \alpha^6 & \alpha^6 & 0 \\ 0 & \alpha^4 & \alpha^4 & \alpha^4 & 0 & 0 & 0 & \alpha^6 \end{pmatrix},$$

$$\rho_{AC_1} = \rho_{C_1B} = \frac{1}{4\alpha^2+4\alpha^6}\begin{pmatrix} 2\alpha^2 & 0 & 0 & 2\alpha^4 \\ 0 & \alpha^2+\alpha^6 & \alpha^2+\alpha^6 & 0 \\ 0 & \alpha^2+\alpha^6 & \alpha^2+\alpha^6 & 0 \\ 2\alpha^4 & 0 & 0 & 2\alpha^6 \end{pmatrix}.$$

$$\rho_{C_1} = \frac{1}{4\alpha^2+4\alpha^6}\begin{pmatrix} 3\alpha^2+\alpha^6 & 0 \\ 0 & 3\alpha^6+\alpha^2 \end{pmatrix}.$$

(III.43)

Interacting Kitaev chain

For the interacting Kitaev chain we can repeat the algorithm used for the Ising chain. In the case of a tripartition we have no differences with the case of the Ising chain, contrary to what happens for the quadripartition. Indeed, taking the quadripartition we have the following reduced density matrices from the even ground-state:

$$\rho_{AC_1B} = \frac{1}{1+6\alpha^4+\alpha^8}\begin{pmatrix} 1 & 0 & 0 & 0 & \alpha^2 & \alpha^2 & \alpha^2 & 0 \\ 0 & \alpha^4 & -\alpha^4 & -\alpha^4 & 0 & 0 & 0 & \alpha^6 \\ 0 & -\alpha^4 & \alpha^4 & \alpha^4 & 0 & 0 & 0 & -\alpha^6 \\ 0 & -\alpha^4 & \alpha^4 & \alpha^4 & 0 & 0 & 0 & -\alpha^6 \\ \alpha^2 & 0 & 0 & 0 & \alpha^4 & \alpha^4 & \alpha^4 & 0 \\ \alpha^2 & 0 & 0 & 0 & \alpha^4 & \alpha^4 & \alpha^4 & 0 \\ \alpha^2 & 0 & 0 & 0 & \alpha^4 & \alpha^4 & \alpha^4 & 0 \\ 0 & \alpha^6 & -\alpha^6 & -\alpha^6 & 0 & 0 & 0 & \alpha^8 \end{pmatrix}$$

$$\rho_{AC_1} = \frac{1}{1+6\alpha^4+\alpha^8}\begin{pmatrix} 1+\alpha^4 & 0 & 0 & \alpha^2+\alpha^6 \\ 0 & 2\alpha^4 & 2\alpha^4 & \\ 0 & 2\alpha^4 & 2\alpha^4 & \\ \alpha^6+\alpha^2 & 0 & 0 & \alpha^8+\alpha^4 \end{pmatrix},$$

$$\rho_{C_1B} = \frac{1}{1+6\alpha^4+\alpha^8}\begin{pmatrix} 1+\alpha^4 & 0 & 0 & \alpha^2-\alpha^6 \\ 0 & 2\alpha^4 & 0 & 0 \\ 0 & 0 & 2\alpha^4 & 0 \\ \alpha^2-\alpha^6 & 0 & 0 & \alpha^8+\alpha^4 \end{pmatrix}$$

and

$$\rho_{C_1} = \frac{1}{1+6\alpha^4+\alpha^8}\begin{pmatrix} 1+3\alpha^4 & 0 \\ 0 & 3\alpha^4+\alpha^8 \end{pmatrix}.$$

(III.44)

In the case of the odd ground state we have:

$$\rho_{AC_1B} = \frac{1}{4\alpha^2+4\alpha^6}\begin{pmatrix} \alpha^2 & 0 & 0 & 0 & \alpha^4 & -\alpha^4 & -\alpha^4 & 0 \\ 0 & \alpha^2 & \alpha^2 & \alpha^2 & 0 & 0 & 0 & \alpha^4 \\ 0 & \alpha^2 & \alpha^2 & \alpha^2 & 0 & 0 & 0 & \alpha^4 \\ 0 & \alpha^2 & \alpha^2 & \alpha^2 & 0 & 0 & 0 & \alpha^4 \\ \alpha^4 & 0 & 0 & 0 & \alpha^6 & -\alpha^6 & -\alpha^6 & 0 \\ -\alpha^4 & 0 & 0 & 0 & -\alpha^6 & \alpha^6 & \alpha^6 & 0 \\ -\alpha^4 & 0 & 0 & 0 & -\alpha^6 & \alpha^6 & \alpha^6 & 0 \\ 0 & \alpha^4 & \alpha^4 & \alpha^4 & 0 & 0 & 0 & \alpha^6 \end{pmatrix},$$

$$\rho_{AC_1} = \frac{1}{4\alpha^2+4\alpha^6}\begin{pmatrix} 2\alpha^2 & 0 & 0 & 2\alpha^4 \\ 0 & \alpha^2+\alpha^6 & \alpha^2+\alpha^6 & 0 \\ 0 & \alpha^2+\alpha^6 & \alpha^2+\alpha^6 & 0 \\ 2\alpha^4 & 0 & 0 & 2\alpha^6 \end{pmatrix}.$$

$$\rho_{C_1B} = \frac{1}{4\alpha^2+4\alpha^6}\begin{pmatrix} 2\alpha^2 & 0 & 0 & 0 \\ 0 & \alpha^2+\alpha^6 & \alpha^2-\alpha^6 & 0 \\ 0 & \alpha^2-\alpha^6 & \alpha^2+\alpha^6 & 0 \\ 0 & 0 & 0 & 2\alpha^6 \end{pmatrix}.$$

$$\rho_{C_1} = \frac{1}{4\alpha^2+4\alpha^6}\begin{pmatrix} 3\alpha^2+\alpha^6 & 0 \\ 0 & 3\alpha^6+\alpha^2 \end{pmatrix}.$$

(III.45)

Having determined the analytical form of all the reduced density matrices, we can proceed to compute the corresponding von Neumann entropies and, finally, the edge-edge squashed entanglement, observing that, again as in the non-interacting case, that the results are insensitive to the choice of the parity as long as we stay on the factorization line and thus take into account the full ground-state degeneracy. Away from the factorization line the degeneracy is removed and the system quickly approaches the boundary separating the topological phase from the trivial phase. In full analogy with the non-interacting case, the quadripartition provides the crucial discrimination between a finite topological edge-edge entanglement in the interacting Kitaev chain and a vanishing end-to-end entanglement in the symmetry-breaking *XYZ* spin-1/2 chain, as shown in Fig. (III.6) below. From the same figure we see that the interaction strongly stabilizes the topological edge-to-edge squashed entanglement almost throughout the entire topological phase.

XYZ CHAIN	INTERACTING KITAEV CHAIN
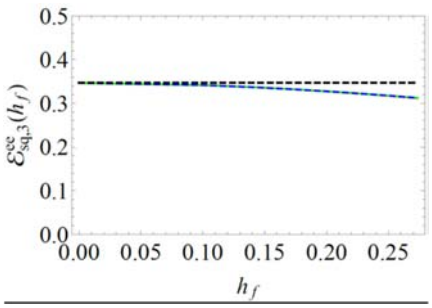 (a)	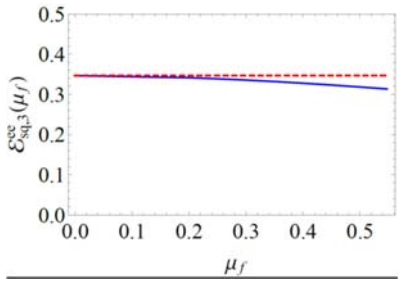
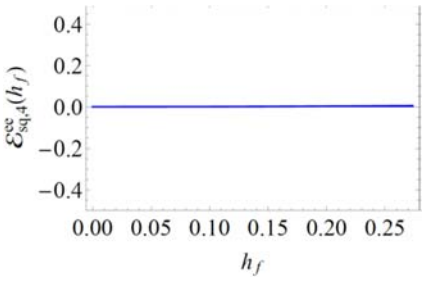 (b)	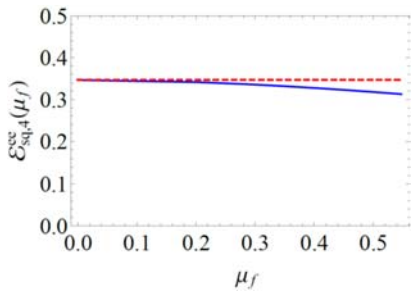

Figure III.6 *Comparison of the edge-edge squashed entanglement in the interacting Kitaev chain vs. the end-to-end entanglement in the XYZ spin-1/2 chain, illustrated for a size of the system L=4. In analogy with the non-interacting case, the edge-bulk-edge leads to no discrimination, while the edge-bulk-bulk-edge quadripartition fully discriminates between the symmetric topological order and the symmetry-breaking Ginzburg-Landau order. In comparison with the non-interacting case, we see that the interaction stabilizes the edge-to-edge entanglement throughout almost the entire topological phase.*

The factorization line ends at the boundary between the topological and the trivial phases, beyond which exact ground-state degeneracy is removed and the edge-to-edge entanglement in the unique ground state (even, for even L) rapidly vanishes at increasing values of the external field.

III.7 Squashed entanglement in 1-D symmetry-protected topological models: Cluster spin chain and its symmetry-breaking counterpart

Another many-body system supporting symmetry-protected topological order in one dimension is the so-called cluster model, i.e. the following quantum spin-1/2 chain with three-site interactions in external field:

$$H_C = -\sum_j \sigma_{j-1}^x \sigma_j^z \sigma_{j+1}^x - h\sum_j \sigma_j^z . \qquad \text{(III. 47)}$$

The Cluster chain has the following features:

- The ground state is exactly 4-fold degenerate at $h = 0$.
- The Hamiltonian is invariant with respect to the symmetry of the group $\mathbb{D}_2 = \mathbb{Z}_2 \times \mathbb{Z}_2$; like the Kitaev chain, the system is symmetry-protected.
- There is a phase transition at $h = 1$ between the topological phase occurring for 0<h<1 and the trivial phase (disordered phase, paramagnetic phase) occurring for h>1.
- The ground-state manifold is spanned by the multipartite entangled cluster states, a generalization of the maximally entangled N-particle GHZ states. The former are of special importance in the measurement-based model of universal quantum computation.

It is instructive to compare the properties of the edge to edge and of the edge to bulk squashed entanglement in the cluster model and in some symmetry-breaking counterpart of the latter, described for instance by the following model Hamiltonian, where the central site in the three-body interaction has been removed:

$$H_{syb} = -\sum_j \sigma_{j-1}^x \sigma_{j+1}^x - h\sum_j \sigma_j^z . \qquad \text{(III. 48)}$$

We have studied the behaviour of the squashed entanglement both in the case of the cluster chain (III.47) and in the case of the symmetry-breaking model (III.48). Both systems possess a four-fold degenerate ground space and this

means that there are four edges: two edges on the first two sites and two edges on the last two sites of the chain with open boundary conditions. As a consequence, we introduce the *(ACB)* tripartition is modified to account for the edge multiplicity, as shown in Fig. (III.7). The corresponding quadripartition (AC_1C_2B) is introduced along the same lines.

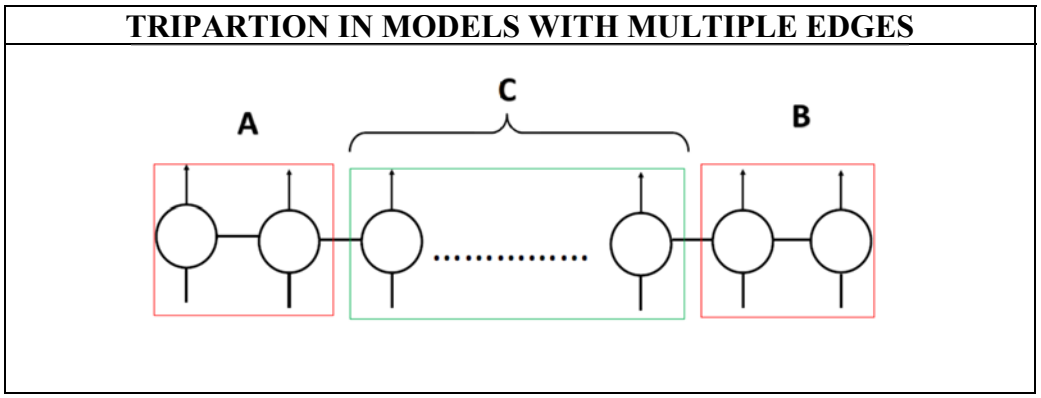

Figure III.7: *Tripartition edge-bulk-edge for a quantum lattice model with two edges on both end sides of a one-dimensional open chain of finite size L.*

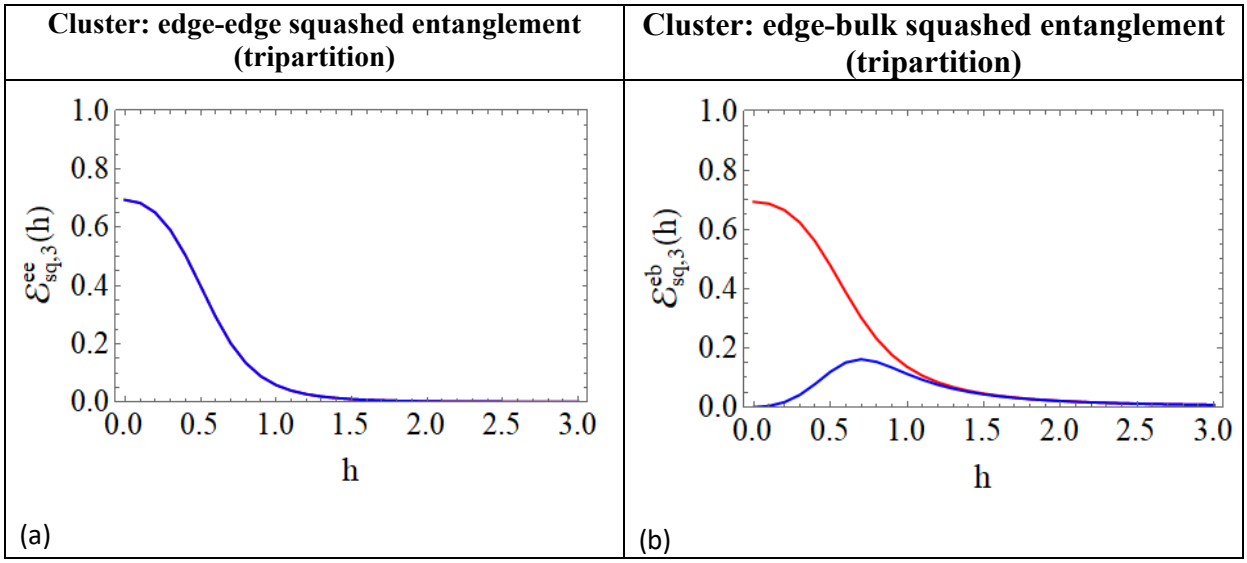

Figure III.8 *Behaviour of the squashed entanglement in the ground state of a cluster spin model and of the corresponding symmetry-breaking counterpart, for a finite open chain of length L = 9. Panel (a): edge-edge squashed entanglement for a tripartition (ACB). No detectable difference between the two models. Panel (b): edge-bulk squashed entanglement in the two models. Blue curve: cluster spin model with symmetry protected topological order: vanishing entanglement. Red curve: symmetry-breaking counterpart with standard Ginzburg-Landau magnetic order. The edge-bulk squashed entanglement discriminates between the two models at the tripartite level, proving the topological nature of the model.*

As shown in Fig. (III.8), panel (a), for a proper edge-bulk-edge tripartition with multiple edges the edge-edge squashed entanglement does not discriminate between the two systems. On the other hand, as shown in Fig. (III.8), panel (b), the edge-bulk squashed entanglement vanishes in the ground state of the cluster spin chain and is finite in the ground state of the symmetry-breaking counterpart, in complete agreement with the previous findings obtained from the comparison between the Ising and the Kitaev chains, and thus proving the (symmetry-protected) topological nature of the 1-D cluster spin model. Extending the analysis to the proper edge-bulk-bulk-edge quadripartition, we find that the edge-edge squashed entanglement discriminates between the two models exactly in the same qualitative form as for the comparison between the Ising and the Kitaev chains, as shown in Fig. (III.8bis) below.

Edge-edge squashed entanglement (quadripartition) Cluster model	Edge-edge squashed entanglement (quadripartition) Symmetry-breaking counterpart
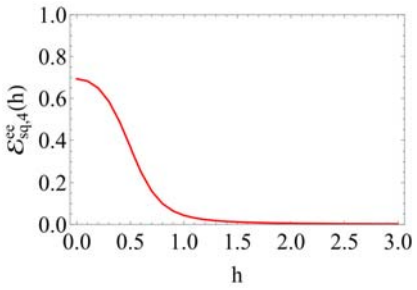 (a)	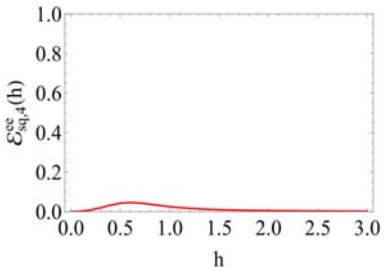 (b)

Figure III.8bis *Panel (a): Behaviour of the edge-edge squashed entanglement for a quadripartition* (AC_1C_2B) *in the ground state of a cluster spin model for a finite open chain of length L = 9. Panel (b): Behaviour of the edge-edge squashed entanglement for the same quadripartition* (AC_1C_2B) *in the ground state of the symmetry-breaking counterpart model for a finite open chain of length L = 9. The edge-edge squashed entanglement is finite throughout the entire topological phase of the cluster spin chain (no edge-bulk correlation), and is vanishing in all phases of the symmetry-breaking counterpart model (non-vanishing edge-bulk correlation); it thus discriminates between the two models and reveals the (symmetry-protected) topological nature of the 1-D cluster spin model, in complete analogy with the previous comparative investigation of the Kitaev fermionic chain vs the Ising spin chain.*

Quantitatively, the maximum finite value of the squashed entanglement in the 1-D cluster spin model (attained at $h = 0$) turns out to be $\ln(2)$, i.e. twice the value attained in the Kitaev chain. As expected, the value of the topological squashed entanglement depends on ground-state topological degeneracy, and

increases with the dimensionality of the edges. Therefore, from the point of view of quantum resource theory, e.g. applied to the problem of topological quantum computation and topological quantum memories, it is desirable to design topological systems with the largest possible edge number, thus maximizing the amount of the topological entanglement resource.

Finally, we have investigated the cluster spin chain with the addition of diamagnetic edges and we have found that they stabilize the Majorana fermions in the ground state and thus the topological squashed entanglement at the constant maximum value *ln(2)* throughout the entire topologically ordered phase ($h < 1$), as shown in Fig. (III.9) below.

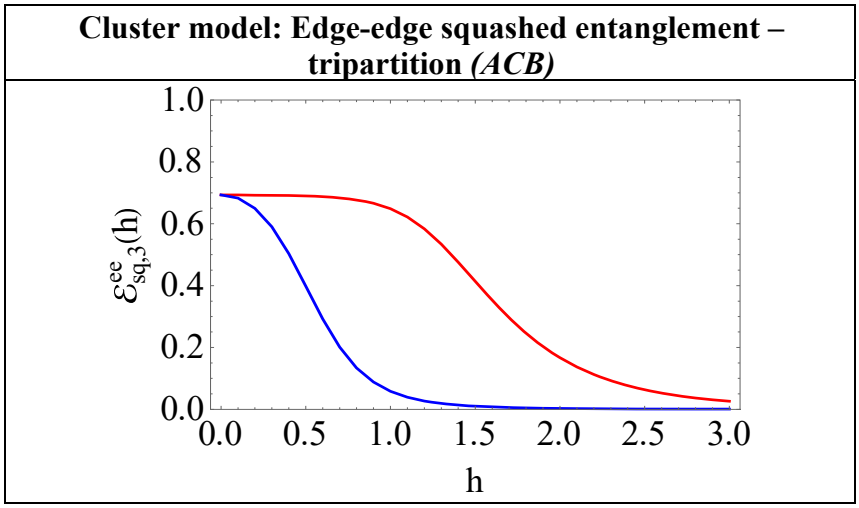

Figure III.9 *Edge-edge squashed entanglement in the ground state of the 1-D cluster spin model on an open chain of size L = 9 as a function of the external field h. Red curve: cluster spin chain with diamagnetic edges; Blue curve: cluster spin chain without diamagnetic edges. The diamagnetic edges stabilize the topological entanglement at the constant maximum value ln(2) throughout the entire topological phase (h < 1).*

III.8 Discriminating topological transitions: Heisenberg-like D-models

It is interesting to discuss the ability of the squashed entanglement to discriminate the transitions to topological order gradually moving to higher dimensions. In this section we consider a class of lattice quantum spin models defined both in one dimension and in sawtooth geometries, a first progression towards ladders, stripes, and finally truly two-dimensional systems. For the class of models that we are going to consider, the very geometrical structure

allows naturally for the unambiguous identification of *(ACB)* tripartitions, which is sufficient to discriminate topological transitions according to the nature of the bulk-edge correlations.

Let us consider the following class of one-dimensional, spin-1 Heisenberg models equipped with double interactions that define the geometric structure shown in Fig. (III.10), and whose Hamiltonian reads:

$$H_D = \sum_{j=1}^{L} S_j^x S_{j+1}^x + D \sum_{j\ odd} S_j^x S_{j+1}^x + h \sum_{j=1}^{L} S_j^z . \qquad \text{(III. 49)}$$

The geometric dimensionality is that of an incomplete ladder with nearest- and next-to-nearest neighbour interactions, the so-called sawtooth chain illustrated in Fig. (III.10) below. This particular class of Heisenberg-like Hamiltonians with two geometrically competing types of interactions is important because it models quasi 1-D structures that actually exist in a wide class of natural materials (e.g., $Cu_2Cl(OH)_3$).

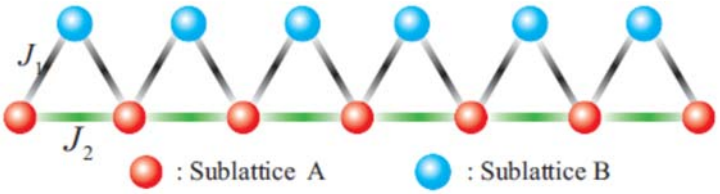

Figure III.10 *Sawtooth open chain lattice of finite size. The two constituent sublattices A and B are endowed with exchange interactions, respectively of strength $J_1 = 1$ and $J_2 = D$, denoted by the grey and the green segments.*

The ruling parameter is the coefficient D of the next-to-nearest neighbour interactions between the odd sites of the lattice (sublattice A). The value $D = 0$ corresponds to an anisotropic spin-1 Heisenberg open chain in external field, admitting a topological phase for sufficiently weak values of the external field h. It is expected that a topological phase should survive also when $D > 0$ up to some critical value D_c to be determined. We have addressed this problem via the edge-bulk squashed entanglement for a tripartite chain that must vanish in a topological phase and attain a finite value otherwise. In Fig. (III.11) we illustrate our results for a chain of length $L = 9$ with $D = 0$, $D = 1/2$, and $D = 6/5$, respectively. We see that indeed the edge-bulk squashed entanglement identifies a topological phase as long as $D \leq D_c \simeq 1.2$. This result is in very good

agreement with the findings of Ref. [27] that combines numerical methods and a handful of experimental results on materials with quasi 1-D structural arrangements.

(A) **Edge-Bulk squashed entanglement (Heisenberg-like sawtooth chain: D = 0)**	**(B)** **Edge-Bulk squashed entanglement (Heisenberg-like sawtooth chain: D = 0.5)**	**(C)** **Edge-Bulk squashed entanglement (Heisenberg-like sawtooth chain: D = 1.5)**
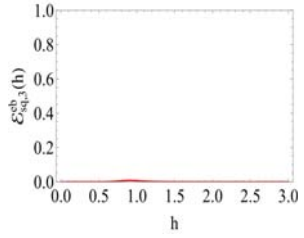	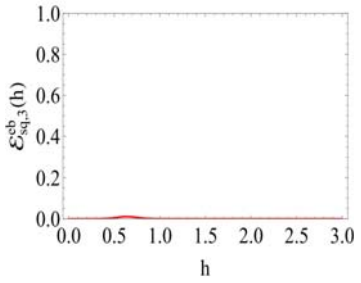	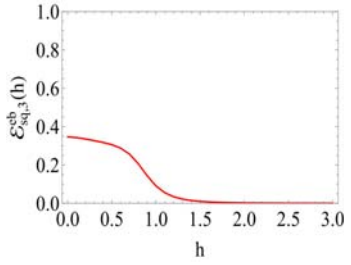

Figure III.11 *Edge-bulk squashed entanglement as a function of the external field h for an Heisenberg-like Hamiltonian, Eq. (III.49), on an open sawtooth chain with L = 9 sites, with an edge-bulk-edge tripartition (ACB), for different values of the sublattice interaction strength D. Panel (A) D = 0.5. Panel (B): D = 0.5. Panel (C): D = 1.5. We see that for a value of D above a critical threshold* D_c *the bulk becomes conducting and gets correlated with the chain edges, barring the onset of a topological phase.*

We have also computed the edge-edge entanglement in all the cases shown above, and verified that it is finite throughout the entire interval *(0 < h < h_c)* for *D < D_c* , proving the existence a *bona fide* topological phase in those regimes. It is worth noticing that the maximum value attained by the squashed entanglement in the topological phase is again $\frac{ln(2)}{2}$ as in the case of the Kitaev chain. This result corroborates the conjecture that the actual value of the squashed entanglement is a simple function of the ground-state degeneracy at the exact topological point. Indeed, also in the case of the Heisenberg-like *D*-models the ground state is exactly two-fold degenerate exactly at $h = 0$.

III.9 Higher-dimensional topological models: preliminary results on the two-dimensional Kitaev toric code

The Kitaev toric code model is defined on a two-dimensional lattice, usually chosen to be the square lattice with periodic boundary conditions, with the spin-1/2 degrees of freedom located on each link between adjacent sites. Stabilizer operators are defined on spin arrangements as stars around each site (or vertex) v of the direct lattice and as closed squares (or plaquettes) centred around each vertex of the dual lattice p of the direct lattice, as follows:

$$A_v = \prod_{i \in v} \sigma_i^x, \qquad \text{(III.50)}$$

$$B_p = \prod_{i \in p} \sigma_i^z \qquad \text{(III. 51)}$$

Where here we use $i \in v$ to denote the links touching the vertex v, and p to denote the edges surrounding the plaquette p. The stabilizer space of the code is that for which all stabilizers act trivially, hence

$$A_v|\psi\rangle = |\psi\rangle, \quad \forall\, v\,; \qquad |\psi\rangle = |\psi\rangle, \quad \forall p. \qquad \text{(III. 52)}$$

On any state $|\psi\rangle$. For the toric code, this space is four-dimensional, and so can be used to store two qubits of quantum information. This can be proven by considering the number of independent stabilizer operators. The occurrence of errors will move the state out of the stabilizer space, resulting in vertices and plaquettes for which the above condition does not hold. The positions of these violations is the syndrome of the code, which can be used for error correction.

The unique nature of the topological codes, such as the toric code, is that stabilizer violations can be interpreted as quasiparticles. Specifically, if the code is in a state $|\phi\rangle$ such that,

$$A_v|\phi\rangle = -|\phi\rangle, \qquad \text{(III. 53)}$$

a quasiparticle known as an e anyon can be said to exist on the vertex v. Similarly, violations of the B_p are associated with so called m anyons on the plaquettes. The stabilizer space therefore corresponds to the anyonic vacuum.

Single spin errors cause pairs of anyons to be created and transported around the lattice.

When errors create an anyon pair and move the anyons, one can imagine a path connecting the two composed of all links acted upon. If the anyons then meet and are annihilated, this path describes a loop. If the loop is topologically trivial, it has no effect on the stored information. The annihilation of the anyons, in this case, corrects all of the errors involved in their creation and transport. However, if the loop is topologically non-trivial, though re-annihilation of the anyons returns the state to the stabilizer space it also implements a logical operation on the stored information. The errors, in this case, are therefore not corrected but consolidated.

Since the stabilizer operators of the toric code are quasi-local, acting only on spins located near each other on a two-dimensional lattice, it is not unrealistic to define the following spin model Hamiltonian for the toric code:

$$H_{TC} = -J\sum_v A_v - J\sum_p B_p\,, -h\sum_i \sigma_i^z\ , \qquad J > 0 \qquad (\mathrm{III}.54)$$

The ground state space of this Hamiltonian is the stabilizer space of the code. Excited states correspond to those of anyons, with the energy proportional to their number. Local errors are therefore energetically suppressed by the gap, which has been shown to be stable against local perturbations. However, the dynamic effects of such perturbations can still cause problems for the code. The gap also gives the code a certain resilience against thermal errors, allowing it to be correctable almost surely for a certain critical time. This time increases with J, but since arbitrary increases of this coupling are unrealistic, the protection given by the Hamiltonian still has its limits that need to be investigated more thoroughly, especially for what concerns the ground-state entanglement, in order to gain a deeper understanding and introduce modifications that allow forms of topological order that might be robust also against thermal fluctuations.

The means to make the toric code, or the planar code, into a fully self-correcting quantum memory is often considered. Self-correction means that the Hamiltonian will naturally suppress errors indefinitely, leading to a lifetime that diverges in the thermodynamic limit. It has been found that this is possible in the toric code only if long range interactions are present between anyons. Proposals have been made for realization of these in the lab. Another approach is the generalization of the model to higher dimensions, with self-correction possible in 4-D with only quasi-local interactions. Here we consider a spin-1/2 toric-code model defined on a two-dimensional lattice as shown in the figure here below:

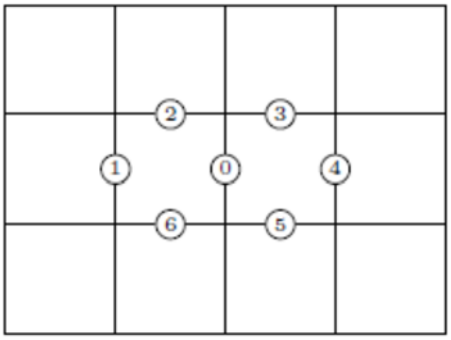

Figure III.12 *A toric-code model defined on a lattice of seven spins 1/2*

In this very preliminary setting, we define the edges as the boundary spins that delimit the area of the lattice covered by the code, which are located on the top and the bottom sides respectively, i.e. the spins 3,2,5,6 in Fig. III.12, while the remaining spins 1,0,4 constitute the bulk. We can then introduce the edge-bulk-edge tripartition *(ACB)* as [edge (2,3)]-[bulk (1,0,4)]-[edge (5,6)]. Proceeding along the same lines illustrated with by the previous one-dimensional examples, we have computed numerically the edge-edge and the edge-bulk squashed entanglement as functions of the external field h. The results are reported in Fig. III.13 below.

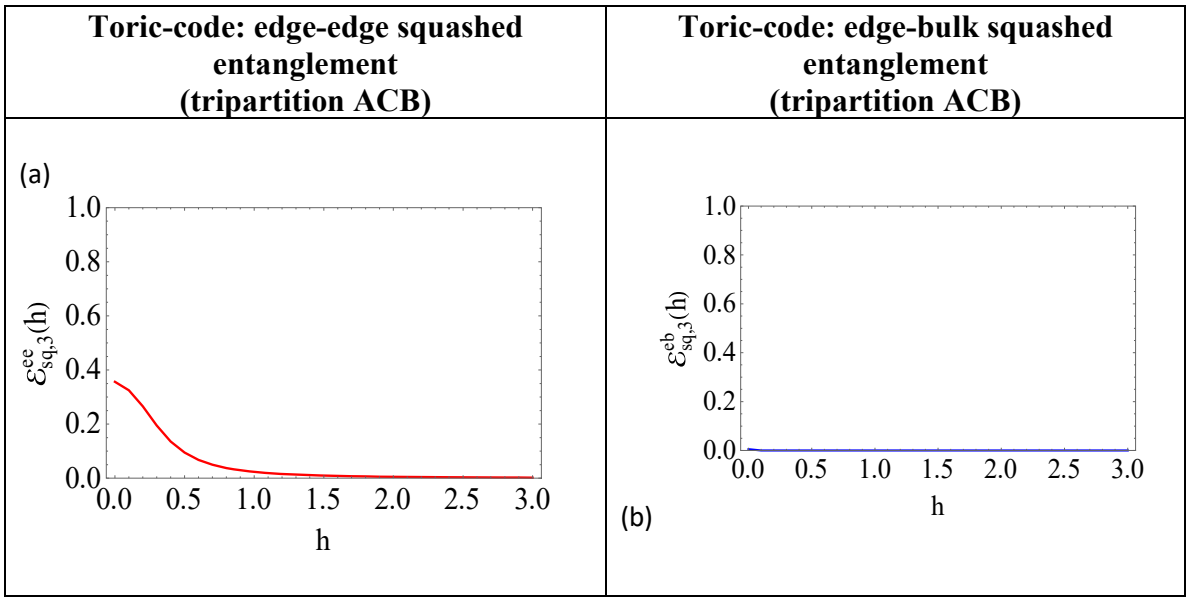

Figure III.13 *Ground-state squashed entanglement for a toric-code Hamiltonian model defined on a two-dimensional lattice of L = 7 spins on the bonds, with periodic boundary conditions. Panel (a): edge-edge squashed entanglement obtained for a canonical edge-bulk-edge tripartition (ACB). Panel (b): edge-bulk squashed entanglement for the same tripartition. We see that the edge-edge entanglement is non vanishing while the edge-bulk entanglement is identically zero, thus corresponding to a bona fide topological phase of the system.*

This very preliminary study seems to indicate that also in 2-D the boundary and boundary-bulk squashed entanglements are able to faithfully characterize the topological nature of certain quantum orders. In the case of the toric code, we see that the edge-edge squashed entanglement is I) non-vanishing in the topological phase (in which anionic excitations are manifest), and II) it is independent of the state of the bulk, as there is no entanglement, and thus no nonlocal quantum correlations, between edge and bulk degrees of freedom.

Introducing diamagnetic edges, we find that the squashed entanglement is stabilised and remains constant in the entire topological phase, as shown in Fig. III.14. The maximum value of the squashed entanglement is set again at $\frac{\ln(2)}{2}$. On the other hand, introducing a diamagnetic bulk has no effect on the entanglement properties of the system: they are indistinguishable from those of the non-diamagnetic case. These findings show once more that the features of

the energy eigenstates of the edges are crucial for the identification and characterization of the system topology. We can conclude that our measure is *bona fide* topological as it depends essentially on the geometry of the system and on the ground state degeneracy. Comparing all the cases investigated so far, it appears that the maximum squashed entanglement (or the squashed entanglement stabilised with diamagnetic edges) takes on two possible values: either 0 in a trivial (disordered) phase or $\frac{n}{2d}\frac{\ln(2)}{2}$ in a topological phase, where n is the ground-state degeneracy and d is the dimension of the space of definition for the lattice geometry.

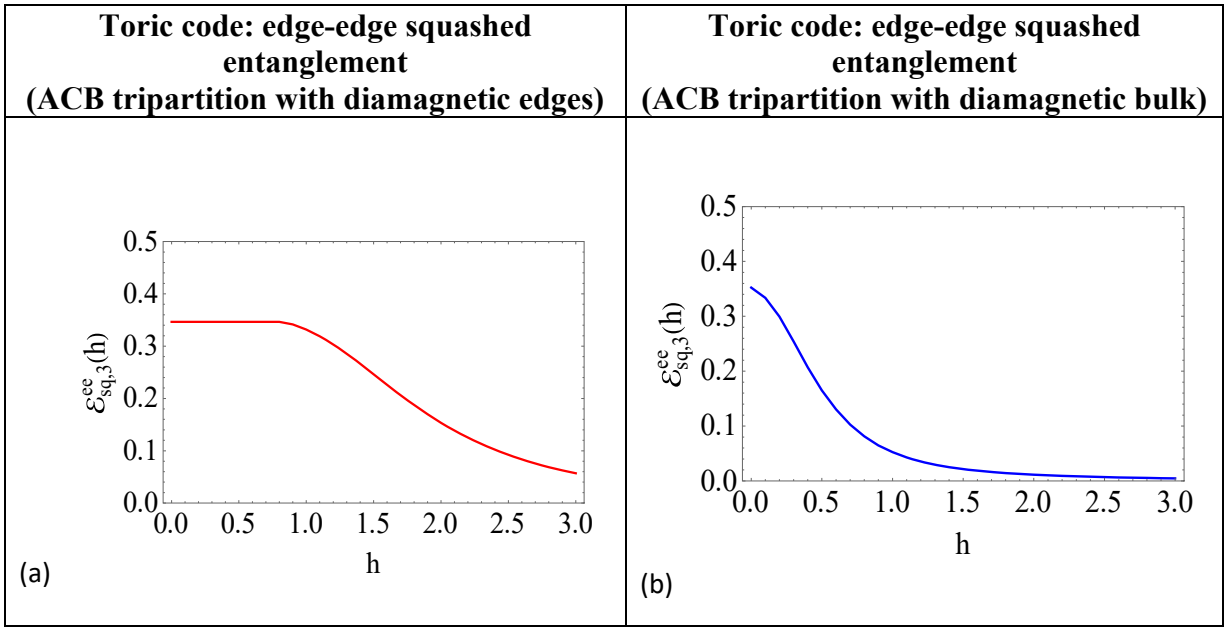

Figure III.14 *Ground-state squashed entanglement for a toric-code Hamiltonian model defined on a two-dimensional lattice of L = 7 spins on the bonds, with periodic boundary conditions. Panel (a): edge-edge squashed entanglement obtained for a canonical edge-bulk-edge tripartition (ACB) and diamagnetic edges. Panel (b): same edge-edge squashed entanglement for the same tripartition, and diamagnetic bulk. We see that the edge-edge entanglement is stabilised by the diamagnetic edges throughout the entire topological phase, while it remains insensitive even to a diamagnetically modified bulk.*

III.10 Enabling and enhancing quantum technologies: edge-edge & edge-bulk tripartition and quadripartition methods

Our results show that every symmetry-breaking system (subject to the interaction of an external field) is distinguished from a topological one by the different properties of the bulk in the ordered (non-trivial) phase that holds for values of the external field below the critical value. In fact, a system that depends on a local order parameter (symmetry-breaking) has a bulk correlated with the edges, while a system that depends on global (topological) features has a bulk with correlation properties different from the edges, and essentially uncorrelated with the latter. Such discriminating traits can be very useful to improve and enhance quantum technologies belonging to the fields of quantum computing, quantum simulation, quantum sensing and cryptography. For example, if we wish to create a transmission line to protect a signal from some noise source, we will need to use a topological material that avoids dispersing this signal during transport and broadcasting, as a topological material will feature a non-conducting bulk. Furthermore, the signal will be transmitted, thanks to the entanglement between the two edges of the cable, faster than non-topological cables are able to. This transmission method can be especially useful for precision measurements relating to magnetic or electric fields.

Vice versa, considering acoustic applications, there is very often the need to purify a signal affected by noise. In this case it would be very useful to have a symmetry breaking material with a bulk related to its edges. Indeed, the signal transmitted in this material is dispersed in the bulk arriving less noisy at the output.

In either case, it will be crucial to identify and characterize the relative edge-edge, edge-bulk, and bulk-bulk properties of different materials and devices in order to specify, design, choose, and optimize the proper ones for each specific technological application. The squashed entanglement appears to be ideally suited for this discrimination and characterization task.

III.11 Future developments

The following developments in flat spaces are either ongoing or planned:

- Introduction of a new basis using edge creation and annihilation operators to track in detail the behaviour of different quantum information measures.

- Introduction of local interaction potentials perturbing Kitaev, Cluster, Ising, and XYZ models in order to assess the robustness of the squashed entanglement in discriminating topological and symmetry-breaking orders;

- Analysis of the effects of integrable and non-integrable potentials on the squashed entanglement.

- Study of bulk and edge correlation proprieties of driven open chains. The driving consists of instantaneous quenches of one-site energy, with main focus of the quasiperiodic modulation of the potentials.

- Study of minimal sets of simultaneous measures able to discriminate different phases, such as von Neumann entropy, mutual information, Schmidt gap, discord, and coherence;

- Definition of a measure that can discriminate models with reciprocal mapping through suitable lattice partitions; definition of finer grained measures able to discriminate between different types of topological orders.

- Development of advanced numerical codes for extensive analysis for models of larger size defined in higher dimensions.

Afterwards we will assess the interplay between topological order and artificial curved geometries aiming at identifying better topological hardware for the next generation of quantum technologies. We plan to:

- Consider spin chains with a site-dependent anisotropy parameter to investigate topological order both at zero and non-zero temperatures;

- Characterize topological spin chains at zero temperature with different bipartite vs multipartite entanglement and coherence measures, and compare them. We also plan to assess the different partitions favouring the chain edges against the chain bulk or vice versa;

- Characterize topological spin chains at non-zero temperature selecting suitable measures such as multipartite Uhlmann fidelity, multipartite coherence measures, and multipartite entanglement measures.

III.12 Papers in preparation

The following papers are in preparation and scheduled to appear soon:

1) F. Illuminati and A. Marino: "*Squashed entanglement: order parameter for topological superconductivity*", preprint in preparation (February 2021).

2) F. Illuminati and A. Marino: "*Purification, squashed entanglement, and bulk-edge correspondence in symmetry-protected topological quantum systems*", preprint in preparation (February 2021).

Chapter 4
CONCLUSIONS AND OUTLOOK

We have identified a specific measure of entanglement, the squashed entanglement, that is able to characterize a topological system and to discriminate it from a symmetry-breaking system such that the two systems can be mapped nonlocally into each other. The understanding of topological proprieties for 1D an 2D systems in flat space can help to highlight the quantum properties in curved space. The latter represent terra incognita and land of promises. Very little is known about quantum systems that are geometrically deformed as if they were coupled to gravity, and even less when the corresponding system in a flat geometry exhibits topological order. Only few isolated studies have considered these problems. For instance, the role of the gravitational anomaly in quantum Hall systems [1], and the gravitational deformation of 1D-spin chains [28]. At the same time, we know that shapes and dynamics of topological defects like vortices strongly depend on the geometry, and that in 2D systems the topological order depends (as in the toric code) on the surface genus. Thus, the topology of the space certainly matters, although many of its effects on many-body systems are mostly unknown and a systematic study is still missing. Coming back to the squashed entanglement and its current and potential future role in the study and understanding of quantum matter, it is important to observe that the squashed entanglement is naturally defined *a priori* on all quantum states, pure or mixed, and in this sense is in the privileged position of being the potentially unique and unifying *prima facie* entanglement measure for the study of quantum matter at zero and finite temperature, and both at equilibrium and in the off equilibrium dynamics (another land that has been only scarcely investigated so far). Finally, the squashed entanglement naturally obeys monogamy inequality relations, and thus its formal extension to a measure of multipartite entanglement both in pure and mixed states is straightforward. As suggested by Prof. Illuminati, multipartite squashed entanglement might thus be the perfect tool for the in-depth investigation of quantum matter going beyond the bipartite layer and into the universe of multipartite, nonlocal quantum correlations. As such, it would be interesting to see whether generalizations of the extension, purification, and squashing procedures can be devised in order to define squashed versions of other quantifiers of quantumness, such as (relative) entropic and geometric measures of Bell nonlocality, as well as measures

of quantum discord and quantum coherence, to develop a unified framework for the hierarchical investigation of quantum correlations and quantum resource theories.

APPENDIX A: ALGORITHMS FOR THE KITAEV CHAIN TRIPARTITION WITH THE RDM TECHNIQUE

We consider the Kitaev chain that is obtained by nonlocally mapping the spin-1/2 degrees of freedom of the Ising chain in spinless fermions. To determine the von Neumann entropies, we use the so-called technique of the reduced density matrix (RDMs) introduced by Peschel [29]. The RDMs have an exponential form of the type e^{-H_A}, whenever H_A is a solvable fermionic or bosonic Hamiltonian related to some subsystem. The method shown here explains how to recover the RDMs grounding all the considerations in the study of correlation functions. Once known the exact spectrum of the RDM, the entanglement entropy follows directly. This technique is available for a quadratic Hamiltonian. We consider the simple case of four sites and we divide the chain in three parts: two edges and the bulk (formed in this case by two sites). In the case of $\mu = 0$, we have two-fold ground states with opposite parity. In particular we consider the ground state with parity P = 1 of the Hamiltonian for L (length of chain) = 4. Now, consider the sites of bulk and we calculate the correlation function $C_{i,j}$ that are defined as:

$$C_{i,j} = \langle \psi_{even} | c_i^+ c_j | \psi_{even} \rangle, \qquad (A.1)$$

Where the indices i and j are the sites of bulk. For the two sites of bulk we have that:

$$C = \begin{pmatrix} \frac{1}{2} & \frac{1}{4} \\ \frac{1}{4} & \frac{1}{2} \end{pmatrix} \qquad (\mathrm{A}.2)$$

Finally, we calculate the correlation function F that are defined as:

$$F_{i,j} = \langle \psi_{even} | c_i c_j | \psi_{even} \rangle \qquad (A.3)$$

For the bulk we obtain the matrix:

$$F = \begin{pmatrix} 0 & -\frac{1}{4} \\ \frac{1}{4} & 0 \end{pmatrix} \qquad (A.4)$$

We determine the following operator:

$$A = \left(C - \frac{I}{2} - F\right)\left(C - \frac{I}{2} + F\right) \qquad (A.5)$$

its matrix form for the bulk is:

$$A = \begin{pmatrix} 0 & -\frac{1}{4} \\ \frac{1}{4} & 0 \end{pmatrix} \qquad (A.6)$$

The eigenvalues of the operator A γ_k are related to the eigenvalues of the subsystem Hamiltonian H_A ϵ_k, by the relation:

$$\epsilon_k = 2arctangh\left(2\sqrt{\gamma_k}\right) \qquad (A.7)$$

The eigenvalues ϵ_k are related to the eigenvalues of RDMs and from exponential form of RDM we obtain that von Neumann entropy has the form:

$$S(\rho_k) = \sum_k -\frac{1}{1+e^{\epsilon_k}} \ln\left(\frac{1}{1+e^{\epsilon_k}}\right) - \left(1-\frac{1}{1+e^{\epsilon_k}}\right) \ln\left(1-\frac{1}{1+e^{\epsilon_k}}\right) \quad (A.8)$$

In the end we obtain:

$$S(\rho_C) = \ln(2). \qquad (A.9)$$

For the $S(\rho_{AC})$ and $S(\rho_{BC})$ the algorithm is analogous and the squashed entanglement is:

$$\varepsilon_{sq,3}^{ee} = \frac{\ln(2)}{2}. \qquad (A.10)$$

For the quadripartition is necessary to apply the same method.

APPENDIX B: CODE ATTACHMENT

A selection of the code written during this work is listed. The code samples represent a small fraction of the total amount of code produced. Still, it is meant to illustrate the diversity of the applied methods for different models treated and the most essential structures needed to reproduce the numerical results.

B.1 Analysis of squashed entanglement for spin chains

In Listing B.1.1 a Mathematica script that analyses the squashed entanglement in different spin chains is provided. This code is the main ingredient used to produce the results in section III, in particular for the spin chains.

```
Lista = {};

Do[



 HFree = H[6, {h, h, h, h, h, h} ];
 SQ = Table[{h, CycleFunction[HFree, 4]} ];
 AppendTo[Lista, SQ];
 Print[h];
 , {h, 0.0, 3.0, 0.1}]
```

Listing B.1.1 *A Mathematica script that analyses the squashed entanglement (SQ) for a spin Hamiltonian (HFree) with six sites in an external magnetic field (h).*

The "CycleFunction" presents in Listing B.1 is a function that takes the Hamiltonian of the system and the bulk sites as input returning the squashed

entanglement of chain partitions. An example of “CycleFunction" for a tripartite chain is reported in Listing B.2

```
CycleFunction[hamiltonian_, NSpinB_] :=
  Block[{Eig, ψB, ψ, ψ1, ψ2, ψ3},
   (*Print["Inizio"];*)

   Eig = Re[Eigensystem[hamiltonian]];

   ψB = SparseArray[N[Chop[Eig[[2, Position[Eig[[1]], Min[Eig[[1]]]][[1, 1]]]]]]]



      ×
     ψ = StateToDensityMatrix[ψB];

   (*ψ=TraceSystem[Normal[ψ],{2,3,4,5,6}];*)
   ψ1 = TraceSystem[Normal[ψ], Table[i, {i, 1, NSpinB + 2}][[1 ;; 1]]];
   ψ2 = TraceSystem[Normal[ψ], Table[i, {i, 1, NSpinB + 2}][[6 ;; 6]]];
   ψ3 = TraceSystem[Normal[ψ], {Table[i, {i, 1, NSpinB + 2}][[1]], Table[i, {i, 1, NSpinB + 2}][[6]]}];
   Return[Re[Squashed[ψ1, ψ2, ψ3]]];
  ];
```

Listing B.1.2 “*CycleFunction”: a script that takes as input the Hamiltonian of spin chain, determines the ground-state (ψ_B) in form of density matrix, computes the different partitions utilizing the Mathematica function “TraceSystem” and finally returns the squashed entanglement with the implemented function “Squashed”.*

B.2 Analysis of squashed entanglement for Kitaev chains

In Listing B.2 a semi-analytic code that analyses the squashed entanglement for Kitaev chains is provided. This code implements in Mathematica the RDM method. The algorithm determines the Kitaev Hamiltonian with a function that takes the chain sites and magnetic field values as input, then it computes the ground-state. To calculate the chain partitions the formulas of the correlation functions (obtained by the RDM method) have been implemented analytically, which have returned the terms of the squashed entanglement. The value of squashed entanglement is obtained taking the minimum between the two values of two-folds ground-states.

Program

```
h = 3.0;

HFree = Hkitaev[6, {h, h, h, h, h, h}       ];

Eig = Re[Eigensystem[HFree]];

v = N[Eig[[2, Position[Eig[[1]], Min[Eig[[1]]]][[1, 1]]]]]
```

```
a = v[[1]];
b = v[[4]];
c = v[[6]];
d = v[[7]];
e = v[[10]];
f = v[[11]];
g = v[[13]];
h = v[[16]];
i = v[[18]];
l = v[[19]];
m = v[[21]];
n = v[[24]];
o = v[[25]];
p = v[[28]];
q = v[[30]];
r = v[[31]];
s = v[[34]];
t = v[[35]];
V = v[[37]];
w = v[[40]];
u = v[[41]];
x = v[[44]];
y = v[[46]];
z = v[[47]];
aa = v[[49]];
bb = v[[52]];
cc = v[[54]];
dd = v[[55]];
ee = v[[58]];
ff = v[[59]];
gg = v[[61]];
```

```
c11 = (a^2 + b^2 + c^2 + d^2 + e^2 + f^2 + g^2 + h^2 + i^2 + l^2 + m^2 + n^2 + o^2 + p^2 + q^2 + r^2);

c22 = (a^2 + b^2 + c^2 + d^2 + e^2 + f^2 + g^2 + h^2 + s^2 + t^2 + V^2 + w^2 + u^2 + x^2 + y^2 + z^2)


c33 = (a^2 + d^2 + f^2 + g^2 + l^2 + m^2 + o^2 + r^2 + t^2 + V^2 + u^2 + z^2 + aa^2 + dd^2 + ff^2 + gg^2);


c12 = (s*i + t*l + V*m + w*n + o*u + p*x + q*y + r*z);

c21 = (s*i + t*l + V*m + w*n + o*u + p*x + q*y + r*z);

c13 = (-t*b - c*V - u*e - z*h - aa*i - dd*n - ff*p - q*gg);
c31 = (-t*b - c*V - u*e - z*h - aa*i - dd*n - ff*p - q*gg);


c23 = (b*l + m*c + o*e + r*h - s*aa - w*dd - x*ff - y*gg);

c32 = (b*l + m*c + o*e + r*h - s*aa - w*dd - x*ff - y*gg);




CC = {{c11, c12, c13}, {c21, c22, c23}, {c31, c32, c33}}


f11 = 0;

f22 = 0;

f33 = 0;
```

```
f21 = (a*aa + b*bb + c*cc + d*dd + e*ee + f*ff + g*gg + h*hh);
f13 = (-a*s - d*w - f*x - g*y - l*bb - m*cc - o*ee - r*hh);
f31 = (a*s + d*w + f*x + g*y + l*bb + m*cc + o*ee + r*hh);

f23 = (a*i + d*n + f*p + g*q - bb*t - V*cc - ee*u - z*hh);
f32 = (-a*i - d*n - f*p - g*q + bb*t + V*cc + ee*u + z*hh);

FF1 = {{f11, f12, f13}, {f21, f22, f23}, {f31, f32, f33}}

FF2 = {{-f11, -f12, -f13}, {-f21, -f22, -f23}, {-f31, -f32, -f33}};
II = {{-1/2, 0, 0}, {0, -1/2, 0}, {0, 0, -1/2}};
a1 = CC + II

a2 = a1 + FF2;
a3 = a1 + FF1;
a4 = a2.a3

gamma1 = Eigenvalues[a4]



eabc11 = 2 * Re[ArcTanh[2 * Sqrt[gamma1[[1]]]]]

eabc12 = 2 * Re[ArcTanh[2 * Sqrt[gamma1[[2]]]]]

eabc13 = 2 * Re[ArcTanh[2 * Sqrt[gamma1[[3]]]]]
```

```
Sabc1 = (-1 / (1 + Exp[eabc13])) Log[1 / (1 + Exp[eabc13])] - (1 - 1 / (1 + Exp[eabc13])) Log[1 - 1 / (1 + Exp[eabc13])] +
  (-1 / (1 + Exp[eabc11])) Log[1 / (1 + Exp[eabc11])] - (1 - 1 / (1 + Exp[eabc11])) Log[1 - 1 / (1 + Exp[eabc11])] +
  (-1 / (1 + Exp[eabc12])) Log[1 / (1 + Exp[eabc12])] - (1 - 1 / (1 + Exp[eabc12])) Log[1 - 1 / (1 + Exp[eabc12])]
```

```
CCac1 = {{c11, c12}, {c21, c22}};

FFac11 = {{f11, f12}, {f21, f22}};

FFac12 = {{-f11, -f12}, {-f21, -f22}};

II2 = {{-1 / 2, 0}, {0, -1 / 2}};

a1ac1 = CCac1 + II2;

a2ac1 = a1ac1 + FFac12;

a3ac1 = a1ac1 + FFac11;

a4ac1 = a2ac1.a3ac1;
```

```
Sac1 = ( -1 / (1 + Exp[eac11])) Log[1 / (1 + Exp[eac11])] - (1 - 1 / (1 + Exp[eac11])) Log[1 - 1 / (1 + Exp[eac11])] +
  (-1 / (1 + Exp[eac12]) Log[1 / (1 + Exp[eac12])] - (1 - 1 / (1 + Exp[eac12])) Log[1 - 1 / (1 + Exp[eac12])])
```

```
gamma2 = Eigenvalues[a4ac1]
```

```
eac11 = Re[2 * ArcTanh[2 * Sqrt[gamma2[[1]]]]]
```

```
eac12 = Re[2 * ArcTanh[2 * Sqrt[gamma2[[2]]]]]
```

```
Sbc1 = ( -1 / (1 + Exp[ebc11])) Log[1 / (1 + Exp[ebc11])] - (1 - 1 / (1 + Exp[ebc11])) Log[1 - 1 / (1 + Exp[ebc11])] +
  (-1 / (1 + Exp[ebc12])) Log[1 / (1 + Exp[ebc12])] - (1 - 1 / (1 + Exp[ebc12])) Log[1 - 1 / (1 + Exp[ebc12])]


gamma4 =  (c22 - 1 / 2) * (c22 - 1 / 2);

ec11  = 2 * Re[ArcTanh[2 * Sqrt[gamma4]]]


Sc1 = (-1 / (1 + Exp[ec11])) Log[1 / (1 + Exp[ec11])] - (1 - 1 / (1 + Exp[ec11])) Log[1 - 1 / (1 + Exp[ec11])]


Sq =  1 / 2 (Sac1 + Sbc1 - Sc1 - Sabc1)
```

Listing B.2 *Kitaev code: a semi-analytic algorithm that computes the squashed entanglement of Kitaev chains utilizing the RDM method.*

BIBLIOGRAPHY

1. T. Can, M. Laskin, and P. Wiegmann, (2014) Phys. Rev. Lett. 113, 046803.

2. N.M. Linke, M.Gutierrez, K. A. Landsman, C. Figgatt,S. Debnath, K. R. Brown and C. Monroe, (2017) Science Advances 3, 1701074.

3. L. Viola, E. Knill, and S. Lloyd, Phys. Rev. Lett. 82, 2417; W. Yang, Z.-Y. Wang, and R.-B. Liu, (2010) Front. Phys. 6, 1; J. R. West, B. H. Fong, and D. A. Lidar, (2010) Phys. Rev. Lett. 104, 130501.

4. G. A. Alvarez, A. Ajoy, X. Peng, and D. Suter, (2010) Phys. Rev. A 82, 042306.

5. K. Khodjasteh and D. A. Lidar, (2005) Phys. Rev. Lett. 95, 180501; K. Khodjasteh and D. A. Lidar, (2007) Phys. Rev. A 75, 062310.

6. M. J. Biercuk, et al., (2009) Nature 458, 996; J. Du, et al., (2009) Nature 421, 1265; G. deLange, et al., (2010) Science 330, 60.

7. C. A. Ryan, J. S. Hodges, and D. G. Cory, (2010) Phys. Rev. Lett. 105, 200402.

8. T. D. Ladd, et al., (2010), Nature 464, 45 (2010).

9. A. Yu. Kitaev, (2001) Phys. Usp. 44, 131.

10. F. Wilczek, (2009) Nat. Phys. 5, 614.

11. J. Alicea, (2012) Rep. Prog. Phys. 75, 076501.

12. M. Leijnse and K. Flensberg, Semicond. (2012) Sci. Technol. 27, 124003 (2012).

13. C. W. J. Beenakker, (2013) Annu. Rev. Condens. Matter Phys. 4, 113.

14. O. Boada, A. Celi, J. I. Latorre and M. Lewenstein,, (2011) New Journal of Physics, 13.

15. Jaeger G, Shimony A, Vaidman L; Shimony; Vaidman (1995) Phys. Rev. 51 (1): 54–67

16. N.M. Linke, M.Gutierrez, K. A. Landsman, C. Figgatt,S. Debnath, K. R. Brown and C. Monroe, (2017) Science Advances , Vol. 3, no. 10, e1701074.

17. L. Viola, E. Knill, and S. Lloyd, (1999) Phys. Rev. Lett. 82, 2417; W. Yang, Z.-Y. Wang, and R.-B. Liu, Front. (2010) Phys. 6, 1; J. R. West, B. H. Fong, and D. A. Lidar, (2010) Phys. Rev. Lett. 104, 130501.

18. T. D. Ladd, et al., (2010) Nature 464, 45.

19. S. D. Bartlett, G. K. Brennen, A. Miyake, (2018) Quantum Sci. Technol. 3, 014010.

20. S. Barik, A. Karasahin, C. Flower, T. Cai, H. Miyake, W. DeGottardi, M. Hafezi, E. Waks, (2018) Science, 359, 666.

21. B. K. Stuhl, H.-I. Lu, L. M. Aycock, D. Genkina, I. B. Spielman, Science (2015): Vol. 349, Issue 6255, pp. 1514-1518.

22. S. Nakajima, T. Tomita, S. Taie, T. Ichinose, H. Ozawa, L. Wan, M. Troyer , Y. Takahashi, (2016) Nature Physics volume 12, 296–300

23. O. Derzhko, (2001) Journal of Physical Studies (L'viv), v. 5, No. 1 49-64.

24. L. Amico, R. Fazio, A. Osterloh, V. Vedral, (2008) Rev. Mod. Phys. 80, 517.

25. P. Calabrese, J. Cardy, (2009) J. Phys. A42, 504005

26. H. Katsura, D. Schuricht and M. Takahashi, (2015) Phys. Rev. B 92, 115137.

27. Y. Yang, S. Ran, X. Chen, Z. Sun, S. Gong, Z. Wang, G. Su, (2020) Phys. Rev. B 101, 045133.

28. H. Ueda and T. Nishino, (2009) J. Phys. Soc. Jap. 78, 014001.

29. I. Peschel and V. Eisler, (2009) J. Phys. A: Math. Theor. 42 504003.

30. M. A. Bandres, S. Wittek, G. Harari, M. Parto, J. Ren, M. Segev, (2018) Science, Vol. 359, Issue 6381, eaar4005

31. L. M. Nasha, D. Klecknera, A. Reada, V. Vitellib, A. M. Turnerc, and W. T. M. Irvine, (2015) Proc. Natl. Acad. Sci. U.S.A. 112, 14495.

32. J. Ningyuan, C. Owens, A. Sommer, D. Schuster, and J. Simon, (2015) Phys. Rev. X 5, 021031.